Postshock turbulence and diffusive shock acceleration in young supernova remnants

A. Marcowith, F. Casse

▶ To cite this version:

Postshock turbulence and diffusive shock acceleration in young supernova remnants

A. Marcowith[1] and F. Casse[2]

[1] Laboratoire de Physique Théorique et d'Astroparticules (LPTA)
UMR 5207 CNRS - Université Montpellier II
13 place E. Bataillon F-34095 Montpellier Cedex 5, France
e-mail: Alexandre.Marcowith@LPTA.in2p3.fr

[2] Laboratoire AstroParticule & Cosmologie (APC)
UMR 7164 CNRS - Université Paris Diderot
10, rue Alice Domon et Léonie Duquet F-75205 Paris Cedex 13
e-mail: fcasse@apc.univ-paris7.fr

ABSTRACT

Context. Thin X-ray filaments are observed in the vicinity of young supernova remnants (SNR) blast waves. Identifying processes involved in the creation of such filaments would provide a direct insight of particle acceleration occurring within SNR, in particular regarding the cosmic ray yield issue.

Aims. The present article investigates magnetic amplification in the upstream medium of SNR blast wave through both resonant and non-resonant regimes of the streaming instability. It aims at a better understanding of the diffusive shock acceleration (DSA) efficiency considering various relaxation processes of the magnetic fluctuations in the downstream medium. Multi-wavelength radiative signatures coming from the SNR shock wave are used in order to put to the test the different downstream turbulence relaxation models.

Methods. Analytical and numerical calculations coupling stochastic differential equation schemes with 1D spherical magnetohydrodynamics simulations are used to investigate, in the context of test particles, the issues regarding the turbulence evolution in both the forshock and post-shock regions. Stochastic second order Fermi acceleration induced by resonant modes, magnetic field relaxation and amplification, turbulence compression at the shock front, are considered to model the multi-wavelength filaments produced in SNRs. γ-ray emission is also considered through the Inverse Compton mechanism.

Results. We confirm the result of Parizot et al (2006) that the maximum CR energies should not go well beyond PeV energies in young SNRs where X-ray filaments are observed. In order to match observational data, we derive an upper limit on the magnetic field amplitude insuring that stochastic particle reacceleration remain inefficient. Considering then, various magnetic relaxation processes, we present two necessary conditions to achieve efficient acceleration and X-ray filaments in SNRs: 1/the turbulence must fulfil the inequality $2 - \beta - \delta_{\rm d} \geq 0$ where β is the turbulence spectral index while δ_d is the relaxation length energy power-law index; 2/the typical relaxation length has to be of the order the X-ray rim size. We identify that Alvénic/fast magnetosonic mode damping does fulfil all conditions while non-linear Kolmogorov damping does not. Confronting previous relaxation processes to observational data, we deduct that among our SNR sample, the older ones (SN1006 and G347.3-0.5) fail to verify all conditions which means that their X-ray filaments are likely controlled by radiative losses. The younger SNRs, Cassiopeia A, Tycho and Kepler, do pass all tests and we infer that the downstream magnetic field amplitude is lying in the range of 200-300 μ Gauss.

Key words. ISM: supernova remnants - Physical data and processes: Acceleration of particle - Magnetohydrodynamics (MHD) - Shock waves - Turbulence - Supernova: individuals: Cassiopeia A - Tycho - Kepler - SN1006 - G347.3-0.5

1. Introduction

Recent Chandra high-angular resolution X-ray observations of young supernova remnants (SNR) as for instance Cassiopeia A, Kepler or Tycho, have revealed the presence of very thin X-ray filaments. They are likely associated with the supernova (SN) forward shock expanding into the interstellar medium (ISM) (Gotthelf et al 2001; Hwang et al 2002; Rho et al 2002; Uchiyama et al 2003; Cassam-Chenaï et al. 2004; Bamba et al 2005a; Bamba et al 2005b; Cassam-Chenaï et al. 2007). The physical properties of these filaments have been reviewed by Vink & Laming (2003), Vink (2004), Weisskopf & Hughes (2006), Ballet (2006), Parizot et al (2006), Bamba et al (2006) and Berezhko (2008). The existence of such filaments is believed to be the result of synchrotron radiation emitted by TeV elec-

trons. The rim-like filaments usually exhibit few arc-seconds angular size as reported in Parizot et al (2006). Their actual width, however has to be inferred from de-projection calculations taking into account the curvature of the remnant (Berezhko et al 2003a; Ballet 2006). It is believed that this size will depend on the magnetic field strength, local fluid properties (the shock velocity and compression ratio) and the relativistic electron diffusion regime.

Recent measurements of the X-ray rim size led to a lower limit on the magnetic field located downstream from the shock front. Typical field strengths two orders of magnitude above the standard ISM values B_∞ have been reported; e.g., Berezhko et al (2003a), Vink (2004), Völk et al (2005), Parizot et al (2006) and Berezhko (2008). Vink (2004) showed that advective and diffusive transports contribute similarly to the filament exten-

sion at high energy close to the electron cut-off. The aforementioned constraints favour value of the electron spatial diffusion coefficient few times larger than the Bohm limit in the downstream region from the shock [1]. These results support the standard scenario of diffusive shock acceleration (DSA) in SNRs and require a strong magnetic field amplification at the shock precursor. However, Chandra observations have been obtained in a limited frequency range. Thus diffusion regimes differing from the Bohm diffusion cannot be ruled out by these sole observations (Marcowith et al 2006). For instance, alternative diffusion regimes may affect high energy particle transport then modifying the way synchrotron spectrum cut-off is reconstructed from the extrapolation of the radio spectrum (Zirakashvili & Aharonian 2007). However recent hard X-ray detection in SNR RXJ1713-3946.5 by Suzaku (Takahashi et al 2008) supports a cut-off spectrum in agreement with a Bohm-like diffusion regime.

The origin of the magnetic fluctuations sustaining the diffusive behavior of non-thermal particles is still widely debated. One possibility is that the turbulent magnetic field is generated by the relativistic particles themselves through their streaming motion ahead of the shock front (Bell & Lucek 2001). The field amplification has strong implications on the physics of cosmic-ray (CR) acceleration at SNRs shocks. For instance, a calculation including the effect of non-linear turbulence transfer has concluded to the possibility of proton acceleration up to the CR spectrum knee at $\sim 3 \times 10^{15} eV$. This calculation was done in the most extreme shock velocity regimes, particularly for SNRs propagating in a hot interstellar medium free of ion-neutral wave damping (Ptuskin & Zirakashvili 2003). Recently, Bell (2004) discussed a non-resonant regime of the streaming instability that can generate a very strong turbulent magnetic field (and boost the CR maximum energy) readily at the very early stage of the SNR free expansion phase. Diamond & Malkov (2007) and Pelletier et al (2006) further insisted on the importance of determining the saturation level of the magnetic fluctuations which was partially discarded in the previous work. Pelletier et al (2006) shown that both resonant and non-resonant regimes of the streaming instability have to be considered simultaneously in order to fix the magnetic field spectrum and strength at the shock front. In fast shocks, the non-resonant instability dominates the magnetic field generation, the level of fluctuation at the shock being found similar to the value derived by Bell (2004). The resonant instability dominates in slower shock regimes. The turbulence generated upstream may then relax downstream from the shock front, producing a limitation of the spatial extension of the non-thermal particle journey (Pohl et al 2005). This possibility has not yet been completely taken into account in the DSA process and the corresponding maximum energy reachable by relativistic particles. This issue is investigated in a dedicated section of the present article. Note that the problem of the maximum CR energy has been addressed recently by Zirakashvili & Ptuskin (2008) using a semi-analytical approach of the non-resonant streaming modes generation. The authors found a maximum CR energy lying between the two confinement limits expected in either a standard ISM medium or in a completely amplified magnetic field. One should keep in mind that several effects may alterate these conclusions as for instance the propagation into a partially ionised medium (Bykov & Toptyghin 2005; Reville et al 2007), thermal effects in the dispersion relation of

the non-resonant instability (Reville et al 2008) or a back reaction on the CR current (Riquelme & Spitkovsky 2009).

While still a matter of debate (see the discussions in Katz & Waxman (2008) and Morlino et al (2008)), the production of relativistic hadrons in SNRs has found observational support in the recent detection of a few TeV γ-ray emitting SNRs in the galactic plane by the HESS telescope. This γ-ray emission may favor the interaction of relativistic hadrons with a dense molecular cloud leading to the Compton up-scattering of low energy photons (Aharonian et al 2004, 2006; Albert et al 2007). Nevertheless, more observations are mandatory before drawing any firm conclusion on this important issue.

The present article aims at investigating issues regarding DSA processes involving magnetic field amplification and relaxation. The paper considers the effect of shock acceleration, spatial variation of the magnetic field (and of the corresponding diffusion coefficient), the possibility of finite diffusive extension zones and the effect of stochastic Fermi acceleration by the electromagnetic fluctuations generated in the shock precursor. This modelling is achieved by means of numerical calculations. The numerical scheme is based upon the stochastic differential equations (SDE) and is described in appendix C. Section 2 presents the general framework adopted in this article. In particular, it investigates the required conditions to develop turbulence upstream from the shock, as expected from the non-linear evolution of the various regimes of the streaming instability. Sections 3 and 4 investigate the impact of post-shock turbulence upon particle acceleration. Section 3 deals with advected downstream turbulence while section 4 refers to a downstream relaxing turbulence. All calculations are then compared to a sample of young SNRs already presented in Parizot et al (2006).
Tab.(1) summarises the notations used in this article (the section where the parameter is reported at first is also indicated).

2. Upstream turbulence generation and accelerated particle diffusion

Highly turbulent supernova shocks involve several complex processes that modify the standard DSA model at some stage of the SNR evolution. In the upstream region, the properties of the turbulence are controlled by the fastest growing instability and its saturation mode (Pelletier et al 2006). The diffusion regime strongly depends on the competition between the wave growth and the energy transfer to other scales provoked by non-linear cascades (Marcowith et al 2006). The turbulence is then compressed at the shock-front; i.e., parallel modes (parallel to the shock normal) do have wavelengths shortened by a factor corresponding to the (sub)shock compression ratio. In the downstream region, the turbulence can either relax (Pohl et al 2005) or be amplified (Pelletier et al 2006; Zirakashvili & Ptuskin 2008). The turbulent magnetic field coherence length may also vary with the distance to the shock, which can be modeled using self-similar solutions (Katz et al 2007).

Section 2.1 recalls the properties of the two regimes (both resonant and non-resonant) of the streaming instability as well as the magnetic field profiles that will be inserted into the coupled SDE-Magnetohydrodynamics (MHD) numerical calculations. In section 2.3 we derive the general form of the diffusion coefficient. Finally, section 2.4 displays the general expression of the particle distribution function, at the shock front, expected in the case of spatially varying diffusive zones. The various expressions derived in this section will be used in sections 3 and 4.

---

[1] The Bohm diffusion coefficient is obtained once the particle mean free path exactly matches its Larmor radius $r_L = E/ZeB$; i.e., $D_{\text{Bohm}} = r_L c/3$.

Turbulence parameters	β	One D power-law spectral index of the turbulence spectrum [Eq.(6)]
	η_T	Level of magnetic fluctuations with respect to the mean ISM magnetic field [Eq.(6)]
	ϕ	Logarithm of the ratio of the maximum momentum to the injection momentum [Eq.(4)]
	λ_{max}	Largest wavelength of the magnetic turbulence spectrum (sect. 2.3)
	ℓ_{coh}	Coherence length of the magnetic fluctuations (sect. 2.3)
	σ	Normalisation factor entering the turbulent spectrum (sect. 2.3)
	$\delta_{u/d}$	Power-law energy dependance index of the relaxation lengths either up- or downstream (sect. 4 and [Eq.(23)]
	H	Ratio of the upstream to the downstream diffusion coefficient at the shock front [Eq.(16)]
	δ_B	Ratio of the resonant to the non-resonant magnetic field strength at the shock front [Eq.(3)]
Relativistic particle parameters	ξ_{CR}	Ratio of the CR pressure to the shock dynamical pressure [Eq.(3)]
	r_L	Larmor radius of a particle (defined using resonant magnetic field)
	ρ	Ratio of the particle Larmor radius to $\lambda_{max}/2\pi$ (also called reduced rigidity, see sect. 2.3)
	E_{CR-max}	Maximal cosmic ray energy (sect. 2.3)
	E_{e-max}	Maximal electron energy (sect. 3.1)
	$E_{\gamma-cut}$	Cut-off synchrotron photon energy emitted by electrons at E_{e-max} (sect. 3.1)
	E_{CR-min}	Injection energy of the cosmic rays (sect. 4.1.4)
	E_{e-obs}	Energy of the electrons producing the observed X-ray filaments (sect. 4.2.4)
SNRs parameters	$V_{sh,4}$	Velocity of the SNR shock wave (in 10^4 km/s unit)
	$B_{d/u,-4}$	Magnetic field amplitude at the shock front respectively in the down- and upstream medium (in 10^{-4} Gauss unit)
	r_B, r_{sub}, r_{tot}	Magnetic, sub-shock and total shock compression ratios (sect. 3.1)
	$\Delta R_{X,-2}$	X-ray filament deprojected width (in 10^{-2} parsec unit, sect. 4.2.4)
Equation parameters	y(r)	$3r^2/(r-1)$ [Eq.(19)]
	K(r,β)	$q(\beta) \times (H(r,\beta)/r + 1)$ [Eq.(36)]
	f$_{sync}$	$H(r,\beta) + r/H(r,\beta)/r_B^2 + r$ [Eq.(39)]
	g(r)	$3/(r-1) \times (H(r,\beta)/r + 1)$ [Eq.(40)]
	C(δ_d)	$(E_{e-max}/E_{e-obs})^{\delta_d}$ [Eq.(41)]

Table 1. Summary of the notations used in this article to denote the various physical quantities and parameters involved in our description of high energy particle yield in supernova remnants (SNR).

2.1. The cosmic-ray streaming instabilities

The streaming instability, provoked by the superalfvenic motion of accelerated energetic particles, generates magnetic fluctuations over a large interval of wave numbers. The resonant instability involves wave-particle interaction at wave scales of the order of the particle gyro-radius r_L (Skilling 1975; Bell & Lucek 2001). The non-resonant regime has been adapted to the SNRs shock waves only recently by Bell (2004); see also Pelletier et al (2006), Zirakashvili & Ptuskin (2008) and Amato & Blasi (2009) for further details. The non-resonant waves are produced, at least in the linear growth phase of the instability, at scales much smaller than r_L. However the ability of the instability to both deeply enter into the non-linear regime and to saturate at a magnetic field level $\delta B \gg B_\infty$ is still a matter of debate (Reville et al 2008; Niemiec et al 2008; Riquelme & Spitkovsky 2009). In the next paragraph, we recall the main properties of the wave modes generated by the non-resonant streaming instability (section (2.1.1)). Then we present the characteristics of the resonant regime in section (2.1.2).

2.1.1. The non-resonant regime

In the linear phase, the most rapidly growing waves have large wave numbers (Bell 2004):

$$k \leq k_c = \frac{j_{cr}B_\infty}{\rho_\infty V_{a\infty}^2 c} \qquad (1)$$

where $j_{cr} = n_{cr}eV_{sh}$ is the current produced by the cosmic rays ahead of the shock wave; n_{CR} is the CR density and V_{sh} is the shock velocity measured in the upstream rest-frame.

The wave number corresponding to the maximal growth rate $\gamma_{max} = k_{up}V_{a\infty}$ is:

$$k_{up} = \frac{k_c}{2} = \frac{n_{cr}}{n_\infty} \times \Omega_{cp} \times \frac{V_{sh}}{2V_{a\infty}^2}, \qquad (2)$$

where n_∞, $\Omega_{cp} = eB_\infty/(m_pc)$ and $V_{a\infty} = B_\infty/\sqrt{4\pi n_\infty}$ are respectively the density, the cyclotron frequency and the Alfvén velocity in the ISM [2].

MHD calculations (Bell 2004; Zirakashvili & Ptuskin 2008) have shown that beyond an exponential growth phase located over a typical scale

$$x_g = V_{sh}/\gamma_{CR-max}$$

---

[2] The density n_∞ is usually the ion density but when the coupling between ion and neutrals is effective it must involve the density of neutrals either

from the shock, the instability enters into a non-linear regime. The magnetic fluctuations are redistributed towards larger scales while the turbulence level evolves in a linearly phase. Bell (2004) and Pelletier et al (2006) discussed several saturation processes all leading to an energy transfer from the dominant wavelength towards large wavelengths (see the discussion in Riquelme & Spitkovsky (2009)). One may then expect the coherence length of the turbulence to be transferred from a scale $\ell_{\text{coh-L}}$ where $k_{\text{max}}^{-1} \leq \ell_{\text{coh-L}} \ll \bar{r}_{\text{L-CR-max}}$ to a scale $\ell_{\text{coh-NL}} < \bar{r}_{\text{L-CR-max}}$ where $\bar{r}_{\text{L-CR-max}} = r_{\text{L-CR-max}} \times B_\infty/\bar{B}$ is the renormalised maximum energy CR gyro-radius in the amplified magnetic field $\bar{B}$. Resonant modes having a harder spectrum (Pelletier et al 2006) contribute to the increase of the coherence length of the turbulence (see section 2.1.2). So, hereafter, we will consider both regimes producing a turbulence with a coherence scale close to $\bar{r}_{\text{L-CR-max}}$; i.e. we neglect the extension of the upstream region where the non-resonant instability is in the linear regime (see section 2.3).

Another important property of non-resonant modes is that they have non-vanishing helicity (Pelletier et al 2006). Indeed, these modes are mostly proton induced and do have a right-handed polarisation with respect to the mean magnetic field far upstream. This non-zero helicity can be the origin of further amplification in the downstream medium where the total magnetic field can eventually reach values close to the equipartition with the kinetic energy of the thermal gas.

2.1.2. The resonant regime

The resonant regime develops simultaneously with the non-resonant regime (Pelletier et al 2006) and *cannot be discarded*. The total amplification factor of the magnetic field $A_{\text{tot}}^2 = B_{\text{tot}}^2/B_\infty^2$ at a distance x from the shock front is a combinaison of both non-resonant and resonant contributions, namely $A_{\text{tot}}^2(x) = A_{\text{NR}}^2(x) + A_{\text{R}}^2(x)$. The exact spatial dependence of $A_{\text{R}}(x)$ is derived in appendix A for completeness. It is found that a good approximation is $A_{\text{R}} \propto A_{\text{NR}}^{1/2}$.
In order to quantify the previous assertion, we can parametrise the contribution of each instability regime. Pelletier et al (2006) argued that the shock velocity is the main controlling factor of the each contribution. This dependence can be deduced from Eq.(A.2). Comparing the respective saturation values of each regimes, one gets:

$$\frac{B_{\text{R}}(x=0)}{B_{\text{NR}}(x=0)} = \delta_{\text{B}} = \left(\frac{\xi_{\text{CR}}c}{V_{\text{sh}}}\right)^{1/4} . \tag{3}$$

While:

$$\frac{B_{\text{NR}}(x=0)}{B_\infty} = \delta_{\text{B}}^{-6} \times \left(\frac{3c^2\xi_{\text{CR}}^4}{\phi V_{\text{A}\infty}^2}\right)^{1/2} . \tag{4}$$

The level of magnetic fluctuations at the shock front given by Eq.(3) and (4) are controlled by δ_{B} and the fraction ξ_{CR} of the SNR dynamical pressure transferred into the CR. The parameter $\phi = \log(p_{\text{max}}/p_{\text{inj}})$ is the logarithm of the ratio of the maximum to the injection momentum and its order of magnitude is approximately between 15 and 16.

As a fiducial example, let us take $\xi_{\text{CR}} = 0.2$, $B_\infty = 4\,\mu$Gauss and set the ion density as $n_{\text{i}} = 0.7\,\text{cm}^{-3}$. We then get three distinct domains:

1. $\delta_{\text{B}} \geq 3$ (corresponding to $V_{\text{sh}} \leq$ c/400): the magnetic field amplification provided by the streaming instability is modest for slow shock velocities.

2. $1 < \delta_{\text{B}} < 3$ (corresponding to c/400 $< V_{\text{sh}} <$ c/10): we get here the ordering $B_{\text{R}} \geq B_{\text{NR}} > B_\infty$ and the ratio $B_{\text{R}}/B_{\text{NR}}$ does not exceed a factor 2.

3. $\delta_{\text{B}} \leq 1$ (corresponding to $V_{\text{sh}} \geq$ c/10): the magnetic ordering becomes $B_{\text{NR}} \geq B_{\text{R}} > B_\infty$. In that case, an upper limit velocity stands close to c. Beyond that limit, the amplification by the non resonant instability is maximal. An accurate analysis is then necessary to compare the saturation of the instability induced by both advection and non-linear effects (Pelletier et al 2009).

Electrons and protons (or ions) moving in the forward or backward direction can resonate with either forward or backward modes. Efficient mode redistribution is expected to produce waves in both direction in the shock precursor (see the appendix of Pelletier et al (2006) for further details). It is noteworthy that the interaction between resonant Alfvèn waves and the shock do produce magnetic helicity different from either +1 or −1 and makes second order Fermi acceleration by the resonant modes unavoidable in the downstream region (Campeanu & Schlickeiser 1992; Vainio & Schlickeiser 1999). This effect will be discussed in section 3.2.

2.2. A note on the evolution of non-resonant modes

Non-resonant modes are purely growing modes having a null frequency, at least in the linear phase. They do not correspond to any normal mode of the plasma as it is the case for the resonant regime. Consequently they are expected to be rapidly damped once the source term is quenched; i.e., at the shock front. The damping length should be of the order of a few plasma skin depths. However, these modes have also a non-vanishing helicity (Pelletier et al 2006; Zirakashvili & Ptuskin 2008) (as we will see in section 4.1.4). So a fraction of the turbulent spectrum can further grow downstream by dynamo action. At this point, the downstream evolution of the non-resonant spectrum is not clear. It may well happen that in some condition the combinaison of magnetic field compression and non-resonant mode damping at the shock front lead to a downstream magnetic field *smaller* than the upstream field, especially in the very fast shock regime (regime 3. discussed in section 2.1.2). This is not the case in the SNR sample considered in this work as the resonant modes tend to be dominant at the shock front. A complete investigation of this difficult issue would require a detailed investigation of the interstellar medium interaction with shocks, in order to fix the ratio $B_{\text{R}}/B_{\text{NR}}$. For this reason we will assume hereafter that the downstream behaviour of the turbulence is dominated by the resonant mode. However, even if $B_{\text{R}}/B_{\text{NR}} > 1$ at the shock front, the fastest growing channel is the non-resonant one and it is essential while considering the complete setting of the magnetic field turbulence in the upstream region. We acknowledge the fact that this assumption weakens the analysis developed in the following sections and consider this first work as an attempt to isolate the main properties of the turbulence around a SNR shock.

2.3. Upstream diffusion regimes

As previously discussed, the most energetic CRs do generate fluctuations at scales much smaller than $r_{\text{L-CR-max}}$. These particles experience a small scale turbulence exclusively in the un-amplified magnetic field. Thus the diffusion coefficient at maximum energy scales as $D(E_{\text{CR-max}}) = (r_{\text{L-CR-max}}/\ell_{\text{coh}})^2 \ell_{\text{coh}}c$ (see next). This allows us to compare x_{g} and $\ell_{\text{diff}}(E_{\text{CR-max}}) = D(E_{\text{CR-max}})/V_{\text{sh}}$, the diffusive length of the most energetic cos-

mic rays. One can then write (Pelletier et al 2006):

$$x_g = \frac{2\phi}{3\xi_{CR}} \times \frac{P_{B\infty}}{\rho_\infty V_{sh}^2} \times \frac{V_{sh}}{V_{a\infty}} \times \frac{\ell_{coh}}{r_{L-CR-max}} \times \ell_{diff}(E_{CR-max}) . \quad (5)$$

We get $x_g \ll \ell_{diff}(E_{CR-max})$ in fast shocks ($V_{sh} > 10^{-2}c$) as $(P_{B\infty}/\rho_\infty V_{sh}^2) V_{sh}/V_{a\infty} \sim V_{a\infty}/V_{sh}$. The following notations have been used to derive the previous result: the CR density is linked to the CR pressure by $n_{CR} = 3P_{CR}/\phi p_* c$ and $p_* = p_{CR-max}$ at a distance $x = \ell_{diff}(E_{CR-max})$ from the shock. The parameter ξ_{CR} is likely to lie between 0.1 and 0.3.

CRs and electrons having energy smaller than E_{CR-max}, diffuse through a large scale turbulence, their transport properties being different from the most energetic CRs (Zirakashvili & Ptuskin 2008). Whatever the turbulence level, the angular diffusion frequency (for a relativistic particle in an amplified field) can be estimated as (Casse et al 2002) (their Eq.A22) :

$$\nu_s \simeq \frac{\pi}{3}\bar{r}_L^{-2} \times (\beta - 1) \times b\, c\, \frac{\delta B^2}{\bar{B}^2} , \quad (6)$$

with

$$b = \ell_{coh} \times \int_{k_{min-NR}\ell_{coh}}^{k_{max-NR}\ell_{coh}} d\ln(k)(k\ell_{coh})^{-\beta} . \quad (7)$$

The turbulence spectrum is assumed to spread over the range $[k_{max}^{-1}, k_{min}^{-1}]$ with a 1D power-law spectral index β. If $\beta = 1$, the term $1/(\beta - 1)$ has to be replaced by a factor $\sigma = \ln(k_{max}/k_{min})$. The corresponding spatial diffusion coefficient is by definition $D = c^2/3\nu_s$. Its energy dependence is related to the development of the instability. In the linear phase (small scale turbulence), we recover the above expression for $\ell_{diff}(E_{CR-max})$. If $k_{min-NR}\ell_{coh} \simeq 1$, introducing the level of turbulence $\eta_T = \delta B^2/\bar{B}^2$, we find

$$D(E) = \frac{\beta}{\pi(\beta - 1)} \times \frac{\ell_{coh}c}{\eta_T} \times \left(\frac{\bar{r}_L}{\ell_{coh}}\right)^2 . \quad (8)$$

In the non-linear phase (i.e. large scale turbulence), we have $k_{min-NR} \sim \bar{r}_L$ and so:

$$D(E) = \frac{\beta}{\pi(\beta - 1)} \times \frac{\ell_{coh}c}{\eta_T} \times \left(\frac{\bar{r}_L}{\ell_{coh}}\right)^{2-\beta} . \quad (9)$$

The results obtained by Casse et al (2002) can be recovered using $\ell_{coh} = \rho_M \lambda_{max}/2\pi$ and adopting a reduced rigidity $\rho = 2\pi \bar{r}_L(E)/\lambda_{max}$. The length $\lambda_{max} \simeq 20\ell_{coh}$ is the maximum scale of the turbulence and ρ_M is a number $\sim 0.2 - 0.3$. This latter number corresponds to the reduced rigidity where the transition between the two diffusive regimes operates. For instance, assuming $\eta_T \simeq 1$ and $\beta = 5/3$, one gets $D \simeq 2.2D_{Bohm}$ at $\bar{r}_L = \ell_{coh}$. This result is consistent with the numerical solutions found by Casse et al (2002). If $\beta = 1$, the energy independent ratio $D/D_{Bohm} = 3\sigma/\pi \simeq 15 - 16$.

We will hereafter refer to $q(\beta)$ as the normalization of the diffusion coefficient such that

$$D(E) = \frac{q(\beta)}{\pi} \times \frac{\ell_{coh}c}{\eta_T} \times \left(\frac{\bar{r}_L}{\ell_{coh}}\right)^{2-\beta} . \quad (10)$$

It is noteworthy that the normalization of the diffusion coefficient is given by $q(\beta)$ and must not be confused with the normalization of the turbulent spectrum. Both quantities appear to have similar expressions as seen from quasi-linear theory calculations or from numerical estimates obtained in Casse et al (2002). Nevertheless, they can differ in a strong turbulence regime. Reville et al (2008) discussed some solutions clearly displaying diffusion coefficient

having sub-Bohm values. This issue is beyond the scope of the calculations done here and are postponed to a future work (see also a recent work by Shalchi (2009)). Considering such uncertainties we consider $q(\beta)$ as a free parameter hereafter.

Pelletier et al (2006) obtained a 1D stationary $\beta = 2$ power-law solution regarding the non-resonant wave spectrum. We see from the above analysis that the energetic particle transport properties around the shock front depend on the possibility for the non-resonant instability to deeply enter into the non-linear regime. Verifying such condition leads to a diffusion coefficient at $E \ll E_{CR-max}$ given by the Eq.(9),the magnetic field profile being characterised by an exponential growth over a scale x_g and a linear growth over a scale $x < \ell_{diff}(E_{CR-max})$.

This qualitative analysis confirms that the non resonant instability contributes to the turbulence level over a large interval of parameters (once the non-linear regime of the instability is established) as well as the control of the turbulence coherence length. The analysis presented in Pelletier et al (2006) shows however that the resonant instability at least in the domain 2 of our fiducial example above also contributes to the magnetic fluctuation spectrum. The resonant wave spectrum is found to be harder; i.e. for a CR distribution spectrum scaling as p^{-4}, the 1D turbulence spectrum has an index $\beta = 1$. In this work a turbulence index lying within the range $1 \le \beta \le 2$ is then admitted.

2.4. Shock particle distribution

Before discussing the effect of turbulence evolution in the downstream region, we present here the general solution of the particle distribution at the shock front in the case of spatially varying diffusion coefficients where radiative losses are discarded. The complete calculation is presented in appendix B. We briefly outline our result (see Eq.B.5) as follows: we have assumed upstream and downstream magnetic fluctuations variation lengths $\ell_{u/d}$ to be scale (or energy) dependent (see section 4). The slope of the stationary particle distribution (neglecting any radiative loss) at the shock front is:

$$\frac{d\ln f_S(p)}{d\ln p} = -\frac{3r}{r-1} \times \left[\frac{D_u(0,p)\exp\left(\int_{-\ell_u}^0 \theta_u(x',p)dx'\right)}{u_u \int_{-\ell_u}^0 \exp\left(\int_{-\ell_u}^x \theta_u(x',p)dx'\right)dx} \right.$$
$$\left. + \frac{D_d(0,p)\exp\left(-\int_0^{\ell_d} \theta_u(x',p)dx'\right)}{ru_d \int_0^{\ell_d} \exp\left(-\int_x^{\ell_d} \theta_d(x',p)dx'\right)dx} \right] \quad (11)$$

The value of the spectrum slope is controlled by the functions $\theta_{u/d} = u_{u/d}/D_{u/d} - d\ln D_{u/d}/dx$ (see Eq.B.3). In the basic case where both upstream and downstream diffusion coefficients can be assumed as space independent over lengths $\ell_{u/d}$ from the shock (and vanishing beyond these distances), the above expression reduced to (Ostrowski & Schlickeiser 1996):

$$\frac{d\ln f_S(p)}{d\ln p} = -\frac{3}{r-1}\left(\frac{r}{1 - \exp(-u_u\ell_u/D_u)} + \frac{1}{\exp(u_d\ell_d/D_d) - 1}\right) . \quad (12)$$

If the shock wave is modified by the CR back-reaction, r will then depend on the particle energy and the shock spectrum will not behave as a power-law. Let us note that provided functions θ are remaining large compared to unity, the previous relation indicates that we will get the standard power-law spectrum expected from DSA theory.

The present article investigates the effects of energy and spatial dependencies of the θ functions both in up- and downstream

regions, relying on a set of available multi-wavelength data of five SNR: Cassiopeia A, Tycho, Kepler, SN1006 and G347.3-0.5 (also known as RXJ 1713-3946.5). All these remnants are in the case 2 discussed in section 2.1.2 and correspond to mildly fast shocks where both resonant and non-resonant magnetic field amplification occur.

3. Particle acceleration in case of downstream advected magnetic field

This section examines the DSA process in the case of an efficient turbulence amplification mechanism producing a large magnetic field in the shock precursor (see section 2). In the first section (3.1), we reconsider the calculations achieved by Parizot et al (2006) but this time including the effect of turbulent scale compression at the shock front. Section (3.2) then addresses the usually overlooked aspect of stochastic particle acceleration in the downstream flow. Finally section (3.3) deals with tests involving the shock solutions obtained recently by Zirakashvili & Aharonian (2007) regarding various turbulent spectrum scaling. We then incorporate particle losses and Fermi stochastic acceleration into the Fermi cycles and proceed to different numerical experiments. We conclude by a comparison between X-ray and γ-ray filaments produced by Inverse Compton up-scattering of cosmic microwave background photons.

3.1. Downstream diffusion regimes and maximum particle energies

Downstream of the shock, the particle distribution has been fully isotropised (to an order of V/v) and the streaming instability is quenched. We insert the magnetic profiles derived in the previous section into the diffusion coefficients (see Eq.9). In order to derive the downstream diffusion coefficients, we need to specify how the transition occurs at the shock front properly. We only consider here the case of a strong magnetic field amplification at the shock precursor. The upstream magnetic field being highly disordered, the magnetic compression ratio then becomes $r_B = \sqrt{(1 + 2r_{sub}^2)/3} \le r_{sub}$ (with $r_{sub} \ge 1$)[3]:

$$B_u = B_d \times \left(\frac{1 + 2\ r_{sub}^2}{3} \right)^{-1/2} = \frac{B_d}{r_B} \,. \qquad (13)$$

Parizot et al (2006) only considered this last effect. But in the meantime, the maximum turbulence scale downstream is reduced by a factor r_{sub}:

$$\lambda_{max-d} = \frac{\lambda_{max-u}}{r_{sub}} \,. \qquad (14)$$

---

[3] We make a distinction between the compression ratio at the subshock ($r_{sub} \le 4$) and the total shock compression ratio $r_{tot} \ge 4$. In the case of weakly modified shocks, we have $r_{tot} \simeq r_{sub} \simeq r = 4$. In the case of strongly CR modified shocks, one gets $r_{tot} > r > r_{sub}$. If the sole adiabatic heating of the precursor is considered, values $r_{sub} = 2-3$ and $r_{tot} > 10$ are possible (see e.g. Berezhko & Ellison (1999)). If a substantial gas heating in the precursor is produced for instance by the absorption of Alfvèn waves, the total compression ratio cannot be much larger than 10, under ISM conditions considered above (Bykov 2004). Whithin strongly modified shock, the most energetic electrons producing the X-ray filaments have energy E $\gg$ E$_{CRmin}$ and do experiment a compression ratio close to r_{tot}. This value will be used in the next estimations. Values of $r_{sub} = 2$ and $r_{tot} = 10$ are accepted in this work in the case of strongly CR modified shock.

This scale compression induces an enhancement of the tangential magnetic field component and a reduction of the maximum turbulence length in the downstream region. The downstream turbulence is then anisotropic, displaying elongated eddies in the direction parallel to the shock front (Marcowith et al 2006) unless other non-linear processes prevail (Zirakashvili & Ptuskin 2008). The coherence length of the turbulence is hereafter assumed as a constant.

We can define the downstream diffusion coefficient accordingly to the definition of the upstream coefficient given in Eq.(9):

$$D_d = \frac{q(\beta)}{\pi} \times \frac{\rho_M \lambda_{max-d} c}{2\pi \eta_{T-d}} \times \left(\frac{\rho_{Ld}}{\rho_M} \right)^{2-\beta_d} \,, \qquad (15)$$

In the rest of the present article, we will only consider the case where $\beta_u = \beta_d = \beta$.

Using Eq.(9) evaluated at $x = 0$ as well as Eq.(13) and (14), we end up linking up- and downstream diffusion coefficients at the shock front (where we have assumed $\eta_T \simeq 1$).

$$D_u = D_d \times r_{sub} \left(\frac{r_B}{r_{sub}} \right)^{2-\beta} = D_d \times H(r_{sub}, \beta) \,, \qquad (16)$$

Once the up- and downstream diffusion coefficients are set, magnetic field at the shock front can be inferred following the same procedure as the one adopted in Parizot et al (2006) (see the article for the detailed derivation). The balance between the electron acceleration rate and the mean synchrotron loss rate fixes the maximum electron energy as $t_{acc}(E_{e-max}) = \langle t_{syn}(E_{e-max}) \rangle$. The synchrotron loss timescale is obtained from Eq.(17) of Parizot et al (2006) using the mean square magnetic field experienced by relativistic electrons during one Fermi cycle:

$$\langle B^2 \rangle = B_d^2 \times \left(\frac{H(\beta)/r_B^2 + r_{tot}}{H(\beta) + r_{tot}} \right) \,. \qquad (17)$$

The acceleration rate is, following DSA standard theory:

$$t_{acc}(E) = \frac{3r^2}{r-1} \frac{D_d(E)}{V_{sh}^2} \times \left[\frac{H(r, \beta)}{r(E)} + 1 \right] \,. \qquad (18)$$

Basic analytical relations can be derived when Bohm diffusion regime prevail. In that case, electron and proton accelerations are no longer related as the diffusion coefficient does not depend on λ_{max} anymore[4]. Eq.(30) in Parizot et al (2006) can be used to derive the downstream magnetic field amplitude and then to give an estimate of the synchrotron photon energy cut-off:

$$E_{\gamma-cut} \simeq [0.875 \text{ keV}] \times \frac{V_{sh,4}^2}{\bar{q}\bar{y}(r_{tot})(1 + H/r_{tot}r_B^2)} \,, \qquad (19)$$

where we have noted $\bar{y}(r_{tot}) = 3\bar{r}_{tot}^2/(r_{tot} - 1)$, $\bar{r}_{tot} = r_{tot}/4$ and $\bar{q} = q(\beta = 1)/16$. The maximum electron energy is found to lie around 10 TeV in our SNR sample, a value close to the maximum CR energy. To derive such result, we have assumed that the compression ratio r at $E = E_{e-max}$ is approximatively $\sim r_{tot}$.

We have listed in Tab.(2) the inferred values of the downstream magnetic field in the context of an advection dominated X-ray rim where a Bohm-type turbulence is occurring. We have also displayed the theoretical values of $E_{\gamma-cut}$ required to verify $t_{acc}(E_{e-max}) = \langle t_{syn}(E_{e-max}) \rangle$. The parameters are the same as in table 1 of Parizot et al (2006) except for SN1006 where we have used an actualized value of the shock velocity (4900km/s) given

---

[4] excepted at the highest energies.

Supernova remnant	B_d (μG)	$\dfrac{E_{\gamma-\text{cut}}}{E_{\gamma-\text{cut,obs}}}$	$B_{d-\text{FII}}$ (mG)
Cas A	558	0.2	2.7
Kepler	433	0.3	2.3
Tycho	586	0.7	1.5
SN 1006	170	0.07	0.56
G347.3-0.5	131	0.05	2.1

Table 2. Inferred values of the downstream magnetic field amplitude and synchrotron photon cut-off energy in the case of an *advection dominated* rim where Bohm diffusion regime prevails ($\beta = 1$ and $q(\beta = 1) = \sigma$). The magnetic field values have been calculated assuming $r_{\text{tot}} = r_{\text{sub}} = 4$. In the last column, the FII magnetic field amplitudes stand for limit values beyond which regular Fermi process is overtaken by the stochastic Fermi process . The surrounding ISM densities are given as approximate and averaged values as follows (in cm^{-3} units): Cas A: $n_\infty = 1$ (Berezhko et al 2003b), Kepler: $n_\infty = 0.7$ (Aharonian et al 2008), Tycho: $n_\infty = 0.4$ (Hughes 2000), SN1006: $n_\infty = 0.05$ (SE rims see Acero et al (2007)), G347.3-0.5: $n_\infty = 1$ (poorly constrained see Aharonian et al (2006)).

in Acero et al (2007). The results presented in this table were performed using a diffusion coefficient normalization $q(\beta = 1) = \sigma$ corresponding to predictions by the quasi-linear theory.

It appears, under the aforementioned assumptions, that older SNRs ($T_{\text{SNR}} > 1000$ yr) would have synchrotron cut-off energy much lower than the observed value. However, as for instance in the case of SN1006, the cut-off frequency depends on the observed region of the SNR and 3 keV is likely an upper limit. On the other hand, young SNRs ($T_{\text{SNR}} < 500 yr$) exhibit, in the same context, large magnetic fields and synchrotron energies cut-off close to the cut-off deduced from the observations. The effect is even stronger in case of modified shocks. Parizot et al (2006) already noticed that the Bohm regime does not allow the DSA theory to reproduce accurately the X-ray filaments unless the diffusion coefficient normalization is replaced by a factor k_0 of the order of a few. This is confirmed by the good agreement between the two cut-off energies obtained for the young SNR.

Several uncertainties may produce shifted cut-off frequency from the extrapolation using the radio data. Zirakashvili & Aharonian (2007) pointed out that the electron particle distribution can be cut off in a smoother way compared to a pure exponential cut-off. In that case the *actual* cut-off frequency is shifted towards higher energies. In the meantime, the observed synchrotron cut-off used previously is likely to be an upper limit because of the back-reaction of CR on the shock structure producing a curved shape of the spectrum. It seems justified to develop a detailed non-linear calculation to improve the estimate of the discrepancy of these solutions with a simple exponential cut-off. This aspect should also be an important issue for the next hard X-ray satellites generation like nuStar or Next. We postponed its investigation to a future work.

As a summary, we can say that the effect of scale compression has a very limited impact on the above calculation and that the results derived in Parizot et al (2006) are found to be quite robust.

3.2. Considering downstream stochastic Fermi acceleration

The downstream magnetic field amplitudes derived in section 3 are actually lower limits while the observed filament sizes are just upper limits because of the lack of resolution of X-ray instruments. If the downstream magnetic field reaches values close to mGauss and does not relax rapidly, then at some stage Alfvén velocity will be of the order of the downstream fluid velocity. In that case, stochastic Fermi acceleration cannot be neglected anymore. Electrons will interact with turbulence modes generated by the resonant streaming instability since non-resonant modes are right-handed polarized and thus cannot interact with elec-

trons. We included in our numerical calculations the so-called Fermi second order process (in addition to the usual first-order acceleration) combined with energy losses, namely synchrotron losses for the electrons. We implicitly assume in our next analysis that an efficient redistribution among forward and backward waves is operating through the interplay of non-linear interaction with magneto-sonic waves (Pelletier et al 2006). In that case, forward and backward modes transmitted downstream are in balance (Vainio & Schlickeiser 1999). Such assumption enables us to estimate the magnetic field amplitude regarding dominant stochastic Fermi acceleration. Issues dealing with imbalanced magnetic turbulence are beyond the scope of this paper and will be investigated in a future work.

The acceleration timescale characterising the stochastic Fermi process for a relativistic particle can be written as:

$$t_{\text{acc,FII}} \simeq \frac{9D(E)}{V_{\text{A,d}}^2} . \tag{20}$$

The condition to get a stochastic acceleration less efficient than the usual shock acceleration can be transposed into a condition on the downstream magnetic field by writing $t_{\text{acc,FII}} \leq t_{\text{acc,FI}}$. Using Eq.(18) and (20) one can easily get that

$$B_{\text{d-FII}} \leq [714\,\mu\text{Gauss}] \times \frac{n_{\infty,-1}^{1/2} V_{\text{sh},3} \bar{r}_{\text{tot}}^{1/2}}{\bar{y}(r)^{1/2}(H(r_{\text{tot}},\beta)/r_{\text{tot}} + 1)^{1/2}} , \tag{21}$$

In this expression we have exceptionally used a shock velocity expressed in units of 10^3 km/s and the ISM density in units of 0.1 cm^{-3}.

In the case of young SNRs propagating into a standard ISM medium with typical hydrogen densities $\sim 10^{-1}$ cm^{-3} the previous limit leads to magnetic field strengths $\sim 1 - 2$ mGauss for typical shock velocity of the order of 5×10^3 km/s. This is confirmed with the estimation of the limited magnetic field strengths given in the table 2 for each SNR. The surrounding gas density in most of the cases is only a crude estimation or is derived from averaged values over the entire remnants (see however the investigation of the gas density around SN1006 by Acero et al (2007)).

The Fermi stochastic acceleration process produces an energy gain in the downstream medium and a hardening of the particle distribution at the shock front (see Eq. 15 in Marcowith et al (2006) and the simulations in section 3.3.2). As particles are continuously reaccelerated downstream, they are expected to produce larger X-ray filaments. Both effects seem clearly incompatible with the available data. The magnetic field fluctuations in resonance with electrons are then expected to saturate at the shock front with magnetic field amplitude $\ll B_{\text{d-FII}}$ below equipartition with thermal pressure of the flow.
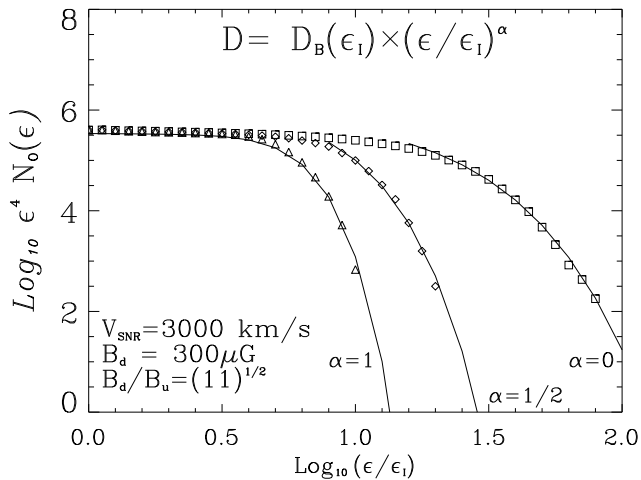
Fig. 1. Shock front energy spectra of relativistic electrons provided by multi-scale simulations where the MHD part of the simulation mimics the behavior of a SNR blast wave (velocity of the downstream fluid 3000 km/s, compression factor $r_{sub} = 4$) and where uniform upstream and downstream magnetic field are set ($r_B = \sqrt{11}$). The numerical spectra are displayed using items while solid lines stand for the analytical spectra cut-off profiles given by Zirakashvili & Aharonian (2007). We have set various diffusion regime ($D \propto E^{\alpha_D}$) while using our new numerical SDE scheme described in appendix C.

3.3. Numerical experiments

The SDE method presented in appendix C does not account for the back-reaction of CR over the fluid flow. This would require a special smoothing and difficult treatment of the CR pressure P_{CR}. The latter calculated from the particle distribution $f(p, r)$ at each grid point would produce unphysical fluctuations that develop with time. Several numerical works have started to included wave generation effects in CR modified shock hydrodynamics (Vladimirov et al 2006; Kang & Jones 2007; Vladimirov et al 2008). Some semi-analytical works have also started to investigate the effect of the wave precursor heating on the CR back-reaction process (Caprioli et al 2008a). Both approaches seem to converge to a similar conclusion: the heating of the precursor by the wave damping reduces the gas compressibility and thus reduces the shock compression (Bykov 2004). Stationary solutions are found to be rather close to the test particle case. Calculations performed in the test particle framework using SDEs can then reproduce the main properties of the particle acceleration process. SDE have several advantages: they are simple to implement and rather simple to couple with MHD equations. SDE schemes enable a fast and large investigation of the parameter space of the DSA mechanism. For instance, the inclusion of Fermi stochastic acceleration is rather simple in the SDE scheme as well as the use of various spatial diffusion coefficient regimes. Our results can, for instance, be used as limiting tests for future non-linear simulations.

3.3.1. Synchrotron spectrum solutions

We first validate the aforementioned numerical scheme by achieving calculations in different configurations, as for instance reproducing the analytical results of Zirakashvili & Aharonian (2007). In this last work, the authors provide the expression of the relativistic electron energy spectra at the shock front in the presence of a discontinuous magnetic field (the discon-
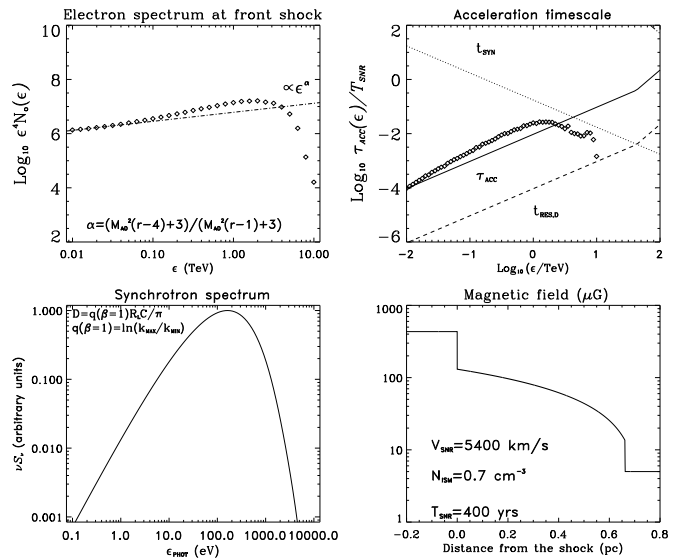

Fig. 2. Energy spectrum of relativistic electrons at the shock front given by MHD-SDE simulations in the conditions of the Kepler SNR (velocity of the upstream fluid is $5.4 \times 10^3 km/s$, compression factor $r_{sub} = 4$) and where uniform downstream magnetic field is set while upstream magnetic field is calculated using results contained within appendix A. The density of ISM is 0.7 cm^{-3}. Bohm diffusion regime has been assumed. The dashed-line shows the stationary solution found in Marcowith et al (2006) which includes particle re-acceleration in the Fermi cycle. In the upper right panel the acceleration (with the sole regular Fermi acceleration), the diffusive and downstream residence timescales are displayed. Diamonds are obtained using a numerical calculation of the acceleration timescale. The slight excess is produced by the stochastic Fermi acceleration process. We also displayed the synchrotron spectrum and the magnetic profile around the shock front at $t = 400 yr$.

tinuity is located at the shock). We have performed several SDE-MHD simulations where constant upstream and downstream magnetic fields prevail ($B_d/B_u = r_B = \sqrt{11}$, r_{sub} is set to 4) and where the shock velocity of the flow is set to 3000 km/s. The various presented simulations differ only from their implemented spatial diffusion coefficients where $D = D_{Bohm}(E_{inf})(E/E_{inf})^{\alpha_D}$ (the particles are injected at energy $E_{inj} = 5$ TeV). Zirakashvili & Aharonian (2007) provided the shape of the electron energy spectra at the shock front beyond the energy cut-off E_{e-max} induced by synchrotron losses, namely $N(E) \propto \exp(-(E/E_{e-max})^{1+\alpha_D})$. Fig.1 displays three simulations with $\alpha_D = 1$ (Bohm diffusion), $\alpha_D = 1/2$ (Kraichnan turbulence) and $\alpha_D = 0$ (constant coefficient). The result of the numerical calculations are displayed using items while analytical solutions of Zirakashvili & Aharonian (2007) are displayed using solid lines. The agreement between numerical calculations and analytical profile is good and proves that the skew SDE numerical scheme is valid for all kind of diffusion regime and can handle magnetic discontinuities properly (see section (C.2.1) for further details).

3.3.2. Shock particle distribution and second order Fermi process

Fig.2 and Fig.3 show the shock particle distribution and synchrotron spectra for the parameters corresponding to the conditions that prevail in the Kepler and G347.3-0.5 SNRs respectively. In the case of Kepler SNR we have used the following pa-
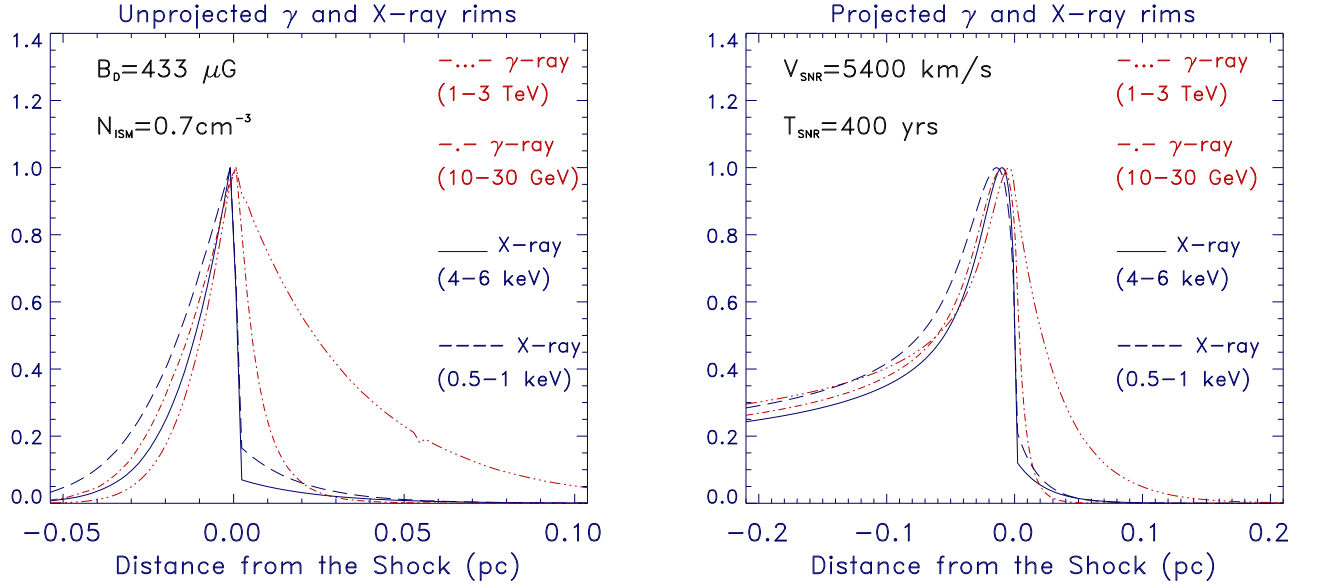
Fig. 4. The unprojected and projected X-ray and γ-ray rims in the conditions of the Kepler SNR (same physical conditions than Fig.2). For clarity both X- and γ-ray rims have been normalized to one.
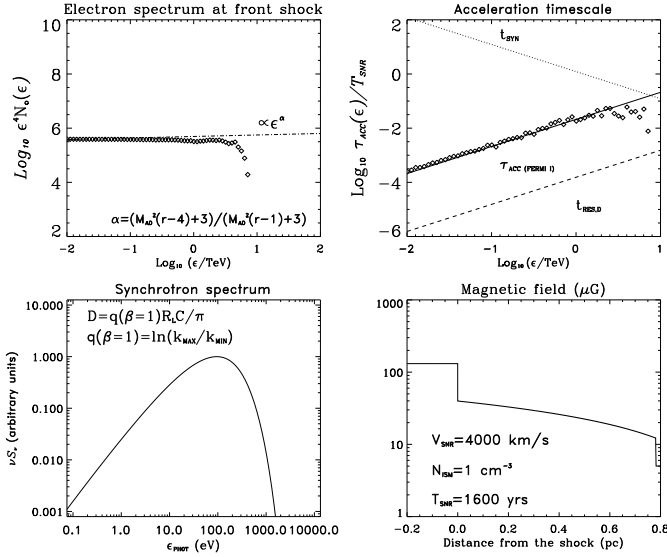

Fig. 3. Same plots than in Fig.2 but in the G347-0.5 SNR (velocity of the shock is $4 \times 10^3 km/s$ and compression ratio $r_{sub} = 4$). The density of ISM is $1 cm^{-3}$. The Bohm regime for the diffusion coefficient has been assumed with $q(\beta = 1) = 15$. The simulation has been performed until time $t = 1600$ years.

The factor χ is usually not well defined. An accurate determination of this parameter requires to perform non-linear simulations of DSA including the effect of the turbulence generation back-reaction on the flow. A fraction of few tenth of percent of the SNR radius is usually assumed in theoretical calculations and seems to be reasonable (Berezhko 1996; Caprioli et al 2008b). The normalization $\bar{\chi} = \chi/0.3$ is then accepted in this text.

It can be seen from Fig.2 and Fig.3 that stochastic acceleration slightly modifies the shock particle spectrum in the case of Kepler SNR. The synchrotron losses create a bump close to the maximum electron energies. In the Kepler remnant, the synchrotron cut-off is found to be around 0.2 keV (see Fig.2) while in the case of G347.3-0.5 it is around 0.5 keV (see Fig.3). We have verified that lowering the normalization factor $q(\beta)$ of the diffusion coefficient from 16 down to 3 produces a cut-off around 1 keV (Kepler) and 2.5 keV (G347.3-0.5), namely a higher cut-off requires a lower $q(\beta)$ (see Eq. 19). The density around G347.3-0.5 is badly constrained and $n_\infty < 1cm^{-3}$ would lead to similar effects. It is noteworthy that the above simulations maximize the incidence of the stochastic acceleration as we considered that the resonant field dominates the total field in the downstream medium (see Eq. 3).

rameters: $V_{sh} = 5.4 \times 10^3$ km/s, $B_d = 433\ \mu G$, $\beta = 1$. Upstream density is $0.7cm^{-3}$ (Berezhko et al (2006) estimated the density $n_\infty \leq 0.7cm^{-3}$). In the case of G347-0.5 we have set parameters as $V_{sh} = 4000$ km/s, $B_d = 131\ \mu G$, $\beta = 1$. The averaged upstream density is $1\ cm^{-3}$ (Aharonian et al 2006). In both cases the magnetic profiles used in the simulations are also presented. The maximum CR energy (and the aspect ratio k_{max}/k_{min}) corresponds to the maximum CR energy limited either by particle escapes in the upstream medium or by the SNR age limit. At E_{CR-max}, the maximal upstream diffusion coefficient allowed by the escaping limit is:

$$D(E_{CR-max}) = \chi \times R_{sh} V_{sh} . \qquad (22)$$

As a conclusion it clearly appears that the downstream Alfvenic Mach number $V_d/V_{A,d}$ cannot be much less than a factor of the order of unity otherwise: 1/ the X-ray filament would be too large with respect to the observed widths (see next section), 2/ the X-ray cut-off frequency would be far larger than $E_{\gamma,cut}$ (see Fig.2) 3/ the radio spectrum would be harder than $\nu^{-0.5}$ (see Fig.2). Generally speaking, the maximum downstream resonant magnetic field cannot be much larger than a few mGauss downstream of the shock front, otherwise regular acceleration process would be dominated by stochastic Fermi acceleration. This set an important constraint on the combined value of the magnetic field and the local ISM density as well as the respective contribution of the resonant and the non-resonant instability to the total magnetic field at the shock front.
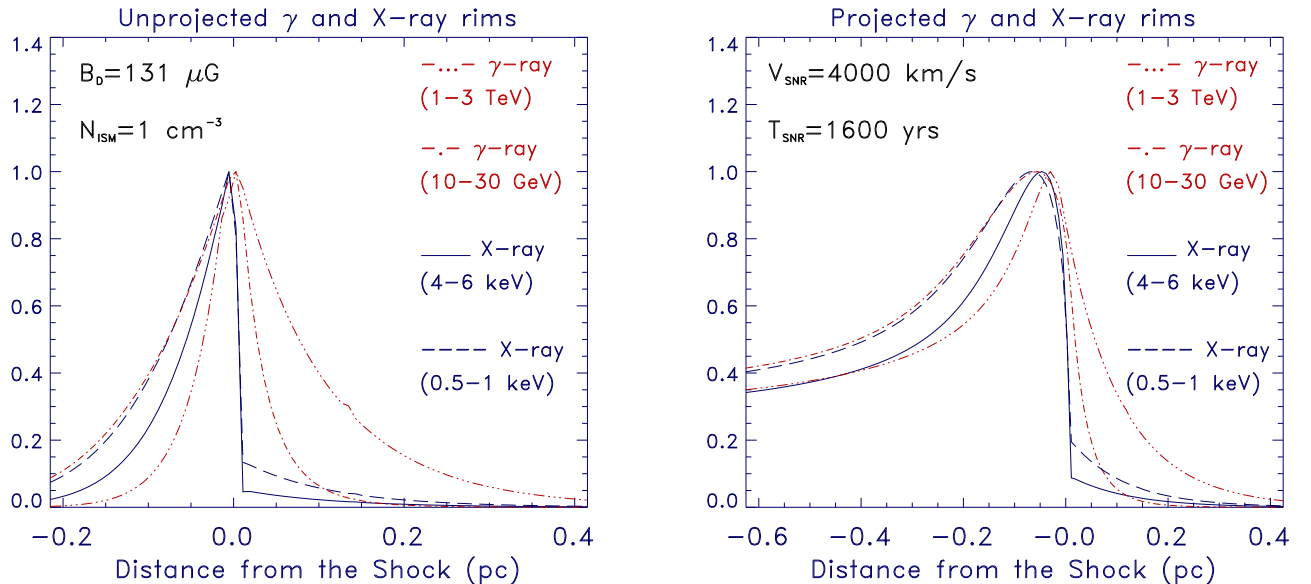
Fig. 5. The unprojected and projected X-ray and γ-ray rims in the conditions of the G347-0.5 SNR (same physical condition than in Fig.3). For clarity both X- and γ-ray rims have been normalised to one.

3.3.3. Comparisons between X- and γ-ray filaments

We end this section by a detailed comparison between X- and γ-ray filaments produced by the relativistic electrons. The inclusion of neutral pion decay that results from the hadronic interaction with the interstellar fluid or with the shocked matter would require a complete modelling of both the hadron spectrum and the ISM density profile around the SNR. Such study is postponed to a future work.

In our calculations, the leptonic γ-ray emission has been integrated in two characteristic wavebands 10-30 GeV and 1-3 TeV using the standard expression of the isotropic Inverse Compton emissivity (Blumenthal & Gould 1970). The rims are produced by the scattering off the cosmic microwave photons with relativistic electrons. They are displayed in Fig.4 and Fig.5 where they were obtained with parameters adapted to the dynamics of the Kepler and the G347-0.5 SNR respectively. We also displayed two X-ray wavebands ($4-6$ keV and $0.5-1$ keV, even if this later wave band is usually dominated by the thermal emission). In each case both projected and deprojected filaments are reproduced. The relative normalization between X-ray and γ-ray filaments mostly depends on the intensity of the magnetic field; it is found to scale for the same particle energy domain as B^2 as expected. The width of the γ-ray TeV rim is usually the largest one as an important fraction of the IC radiation is produced upstream. The $10-30$ GeV γ-rays are produced closer to the shock upstream comparing to $1-3$ TeV γ-rays. In the downstream region, the the highest energetic electrons are confined closer to the shock because of their shorter radiative loss timescales. The projected rims show that only a slight difference exists between the position of the peak of the gamma and X-ray emission. As the size of the γ-ray rims is actually not much larger than the X-ray filaments, it seems impossible for any actual γ-ray instrument to separate both components. This will be also the case for future instruments like CTA unless the filaments being very large (see the case of Vela Junior discussed in Bamba et al (2005a)).

4. Diffusive shock acceleration in case of downstream spatially relaxing turbulence

In this section, we will now consider a scenario where the downstream magnetic field fluctuations vary over a length-scale much shorter than the SNR shock radius R_{SN}. This scale noted ℓ_d can depend on the wave number k of the fluctuations. The damping of the turbulence in the downstream medium and its compression at the shock front can modify the particle mean residence time and the relativistic particle return probability to the shock. Hence such magnetic relaxation is expected to modify the efficiency of the diffusive acceleration process itself.

Equation (12) shows that the particle energy spectrum at the shock front remains a power-law provided quantities (at a given energy E) $z_{u/d}(E) = u_{u/d}\ell_{u/d}/D_{u/d}$ are large compared to unity. Having $z_{u/d}(E) \leq 1$ will produce a strong softening of the particle distribution and a drop off of the acceleration timescale, the latter being dominated by the particles experimenting the shortest residence time. A softening effect induced by the upstream losses is only expected at highest energy near E_{CR-max}, namely once $z_u \to 0$ [5]. The diffusive length of particles having energy smaller than E_{CR-max} is always smaller than the variation scale of the magnetic fluctuations ℓ_u (controlled by the highest energy), hence we have $z_u(E < E_{CR-max}) \gg 1$, leading to a vanishing exponential factor in the above solution. Conversely, the softening effect downstream can be significant at energies much smaller than E_{CR-max} as ℓ_d can be highly scale (and thus energy) dependent. This is precisely the main topic of this section, namely trying to identify the parameter space that allows the Fermi acceleration process to be efficient in the context of a relaxing downstream turbulence.

Hereafter the downstream relaxation length ℓ_d is considered to be energy dependent and we normalize it with respect to the maximum CR energy; E_{CR-max}:

$$\ell_d(E) = \ell_{d,M} \times \left(\frac{E}{E_{CR-max}}\right)^{\delta_d} = \ell_{d,M} \times \left(\frac{k_{min}}{k}\right)^{\delta_d}. \quad (23)$$

---

[5] Again, a correct way to handle this effect requires to account properly for the particle back-reaction on the flow.

The scale $\ell_{\rm d,M}$ is the relaxation scale at the maximum particle energy [6]. Let us recall that the relationship between energy particle and wave vector comes from the condition for a given particle to resonate with a turbulence mode, $kr_L \sim 1$. In this section, we first investigate the magnetic field profiles in the downstream medium resulting from various relaxation processes (Section 4.1). In Section 4.2 the efficiency of the DSA with respect to the turbulence properties (turbulence index, relaxation index) is discussed, in particular concerning the effect of the downstream magnetic field amplitude. Various numerical experiments, presented in Section 4.3 illustrate the effect of the magnetic field spatial variation on the particle dynamics and the associated X- and γ-ray rims.

4.1. Downstream magnetic field relaxation

This work considers various turbulent magnetic field damped profiles: the case of an energy dependent Heaviside profile, the profile produced by a non-linear Kolmogorov-type damping (Ptuskin & Zirakashvili 2003) and the profile produced by the Alfvén or fast magnetosonic cascades (Pohl et al 2005). We also briefly discuss the case of a turbulent dynamo action downstream (Pelletier et al 2006). In this section unless specified $\delta_{\rm d} \geq 0$ is implicitly assumed.

4.1.1. Heaviside profiles

Heaviside-type magnetic relaxation accounts for an idealized approach of turbulence relaxation where a given turbulence mode is assumed to be uniform up to a distance $\ell_{\rm d}(k)$ from the shock and to vanish beyond that distance. This relaxation model is very likely to be unphysical but it enables to catch the basic features of the turbulence relaxation effects upon particle acceleration. Assuming such profile, we write the magnetic energy turbulence spectrum as (the downstream medium is defined by $x > 0$):

$$W(k,x)_{\rm d} = W(x=0^+,k)\Pi(\ell_{\rm d}(k)-x) + W_\infty\Pi(x-\ell_{\rm d}(k)) \quad (24)$$

where Π functions are Heaviside functions and x is the distance from the shock front. The magnetic energy density far downstream is W_∞. The normalization of the turbulent spectrum $W(k) = W_0\bar{k}^{-\beta}$ is related to the magnetic field at the shock front through $W_0 = B^2(x=0^+)/4\pi\sigma k_{\rm min}^{-1}$, with $k_{\rm min} = 2\pi\lambda_{\rm max,d}^{-1}$, $\bar{k} = k\lambda_{\rm max,d}$ and again $\sigma(\beta=1) = \ln(k_{\rm max}/k_{\rm min})$ and $\sigma(\beta>1) \simeq 1/(\beta-1)$.

The Heaviside profile, despite it crudely approximates the variation of the magnetic energy density downstream, permits us to derive a basic spatial profile of the total magnetic field as given by

$$\frac{\delta B^2(x)}{4\pi} = \int_{k_{\rm min}}^{k_{\rm max}} W(k,x)dk \quad (25)$$

which, for instance in the case of a Bohm turbulence leads to (ℓ_{min} is defined as $\ell_{\rm d,M} \times (k_{min}/k_{max})^{\delta_d}$)

$$0 < x \leq \ell_{\rm min} \;\; : \;\; \frac{\delta B^2(x)}{4\pi} = \frac{\delta B^2(0^+)}{4\pi} + \frac{\delta B_\infty^2}{4\pi}$$

$$\ell_{\rm min} \leq x \leq \ell_{\rm d,M} \;\; : \;\; \frac{\delta B^2(x)}{4\pi} = \frac{\delta B^2(0^+)}{4\pi}\frac{\ln(\ell_{\rm d,M}/x)}{\delta_d \ln(k_{\rm max}/k_{\rm min})} + \frac{\delta B_\infty^2}{4\pi}$$

$$\ell_{\rm d,M} \leq x \;\; : \;\; \frac{\delta B^2(x)}{4\pi} = \frac{\delta B_\infty^2}{4\pi} \quad (26)$$

[6] All quantities with an index M are to be taken at the maximum particle energy.

At any given downstream location $\ell_{\rm d,M} \geq x \geq \ell_{\rm min}$, the maximum non-vanishing turbulence wave number is $k_{\rm max}(x) = k_{\rm min}(\ell_{\rm d,M}/x)^{1/\delta_{\rm d}}$. Beyond $\ell_{\rm d,M}$, all turbulent modes vanish giving a total magnetic field B_∞ close to the ISM magnetic field value. The spatial variation of the magnetic field for any other diffusion regime is more complex, as it scales as $1 - (\ell_{\rm d,M}/x)^{(1-\beta)/\delta_{\rm d}}$ for $x \geq \ell_{\rm min}$. The total magnetic field is required to calculate the synchrotron losses properly but also the normalization entering the particle Larmor radius and the local Alfvèn velocity. Once total magnetic field is known, we can calculate, for every relativistic particle having energy E, what is the fraction of the total magnetic field that can resonate with this particle, namely integrating all turbulence modes verifying $1/\bar{r}_L(E) \leq k \leq k_{\rm max}(x)$. This is done by computing the function b defined in Eq.(7). If magnetic turbulence relaxation follows a Heaviside prescription then one obtains:

$$b(0 < x \leq \ell_{\rm min}, E) \simeq \frac{\ell_{\rm coh}}{\beta}\left(\frac{\bar{r}_L(E)}{\ell_{\rm coh}}\right)^\beta \quad (27)$$

$$b(x \geq \ell_{\rm min}, E) = \frac{\ell_{\rm coh}}{\beta}\left\{\left(\frac{\bar{r}_L(E)}{\ell_{\rm coh}}\right)^\beta - \left(\frac{\bar{r}_L(E_{\rm CR-max})}{\ell_{\rm coh}}\right)^\beta \left(\frac{x}{\ell_{\rm d,M}}\right)^{\beta/\delta_d}\right\}$$

Once both the total magnetic field and function b are known, it is easy to compute in our simulations both spatial and energy diffusion coefficients for every test particle which are mandatory to get the particle motion and stationary particle distribution solutions in Eq.(11) and Eq.(B.2). The procedure is repeated in the same way for any magnetic profile.

4.1.2. Non-linear Kolmogorov damping

In models of incompressible MHD turbulence described by the Kolmogorov energy cascade towards the large wave numbers, the non-linear damping kernel scales as $k^{5/2}W(k)^{3/2}$. Following Ptuskin & Zirakashvili (2003) this kernel can be simplified while still respecting the spatial relaxation profile. We have:

$$\Gamma_{\rm NL}(k,x) \simeq \Gamma_0 \times k^{3/2}W(k,x)^{1/2} , \quad (28)$$

where $\Gamma_0 \simeq 5 \times 10^{-2} \times V_{\rm a,d}/(B_{\rm d}^2/4\pi)^{1/2}$. Here we consider the cascade to be initiated behind the shock and use the local total magnetic field and Alfvén velocity.

In the shock rest-frame, the turbulence relaxation downstream (for $x > 0$) is described by a stationary equation:

$$\frac{V_{\rm sh}}{r_{\rm tot}} \times \frac{\partial W(k,x)}{\partial x} = -2\Gamma_{\rm NL}(k,x)W(k,x) , \quad (29)$$

and a boundary solution $W(k, x = 0^+) = W_0 \times \bar{k}^{-\beta}$. The solution of Eq.(29) is:

$$W(k,x) = \frac{W(k,x=0^+)}{\left(1 + \bar{k}^{(3-\beta)/2}\dfrac{x}{x_0}\right)^2} . \quad (30)$$

An estimate of the scale x_0 is (see Pohl et al (2005)):

$$x_{0-{\rm K}} \simeq [300 \times \lambda_{\rm max,d}] \times \frac{V_{\rm sh,4}n_\infty^{1/2}\bar{r}_{\rm sub}^{1/2}\bar{\sigma}^{1/2}}{\bar{r}_{\rm tot}} \times B_{\rm d,-4}^{-1} . \quad (31)$$

We used $\bar{\sigma} = \sigma/16$ and the shock velocity $V_{\rm sh,4}$ is expressed in units of 10^4 km/s. The downstream maximum turbulence scale $\lambda_{\rm max,d}$ can be connected to the maximum Larmor radius of CRs upstream through Eq.(14). Reduced rigidity at maximal energy

E_{CR-max} is such that $\rho_{Lu} \simeq \rho_M$ as the diffusion coefficient rapidly increases as E^2 beyond E_{CR-max}. Both conditions set the maximum upstream turbulence scale $\lambda_{max,u}$ and the maximum CR energy E_{CR-max}. We find $\lambda_{max,d} \simeq 5.2\, r_{L-max,u}/\bar{r}_{sub}\bar\rho_M$, where $\bar\rho_M = \rho_M/0.3$.

The relaxation scale is $\ell_d(E) = \ell_{d,M} \times (E/E_{CR-max})^{(3-\beta)/2}$. The factor $\ell_{d,M}$ is defined as the length on which turbulence level has decreased of $1/e$ compared to its value at the shock front; i.e. $\ell_{d,M} = (\sqrt{e} - 1)x_0$. The spatial dependence of the total magnetic field and function b have been calculated using Eq.(25) and Eq.(7). These expressions, rather tedious especially for the b function in the Eq.(6), have been implemented into the code but are not explicitly given here.

4.1.3. Exponential profiles

When turbulence damping rate does not depend on space but remains dependent on wave number ($\Gamma = \Gamma(k)$), the relaxation of the downstream magnetic field follows an exponential cut-off on a scale length $\ell_d(k) = r_{tot}\Gamma(k)/V_{sh}$. The turbulent magnetic energy spectrum is then

$$W(k,x) = W(k,0^+) \times \exp\left(-\frac{x}{\ell_d(k)}\right) \tag{32}$$

The Alfvén and Magnetosonic waves cascades considered by Pohl et al (2005) follow this scaling, the corresponding damping rates and expression for x_0 can easily be obtained from their Eq. (8) and (11) respectively. Considering the Alfvenic cascade, we obtain

$$x_{0-A} \simeq \left[\bar\rho_M^{1/2} \times \lambda_{max,d}\right] \times \frac{V_{sh,4}n_\infty^{1/2}\bar{r}_{sub}^{1/2}}{\bar{r}_{tot}} \times B_{d,-4}^{-1}. \tag{33}$$

The coherence scale of the downstream turbulence is $\ell_{coh} = \lambda_{max,d}\,\rho_M/2\pi$. The fast magnetosonic cascade leads to a similar expression except that the wave phase velocity can be approximated as $V_{FM,d} = (V_{A,d}^2 + c_{s,d}^2)^{1/2}$, $c_{s,d}$ being the sound velocity behind the shock front. Notice that the above expression for the Alfvén cascade results from the combinaison of the critical balance and the anisotropy obtained in the Goldreich-Sridhar phenomenology of strong turbulence (Goldreich & Sridhar 1995). Again, the expressions of the total magnetic field and resonant field are rather tedious and are not given here. It is noteworthy that Eq. (31) and (33) show that the Kolmogorov damping leads to slower cascade timescales and thus to larger relaxation scales than for an exponential damping.

4.1.4. Turbulent dynamo downstream

Pelletier et al (2006) (see also Zirakashvili & Ptuskin (2008)) discussed the action of a turbulent dynamo in the downstream medium that would lead to a further amplification of the magnetic field. The magnetic field is expected to saturate at value close to equipartition with the dynamic gas pressure. The dynamo action is driven by the non-vanishing helicity of the non-resonant turbulent modes.

The corresponding scale of magnetic field variation is given by the ratio of the magnetic turbulent diffusivity ν_t to the dynamo amplification coefficient α_D. The two coefficients can be expressed as (Pelletier et al 2006):

$$\alpha_D \simeq \frac{2c}{3\pi} \times \left(\frac{\bar{V}_a}{V_{sh}}\right)^2 \times \ln\left(r_L\left(E_{CR-Max}\right)/r_L\left(E_{CR-min}\right)\right), \tag{34}$$

and

$$\nu_t \simeq \frac{2c\lambda_{max,d}}{3\pi^2} \times \left(\frac{\bar{V}_a}{V_{sh}}\right)^2. \tag{35}$$

E_{CR-min} stands for the smallest resonant energy. Then the amplification scale is $\ell_{ampl} \sim \lambda_{max,d}/(\pi\phi)$. Turbulence modes having wavelength larger than ℓ_{ampl} grow and saturate close to the equipartition. Other turbulence modes are expected to damp rapidly (over a few plasma skin depths) because the non-resonant waves are not normal modes of the plasma, as already stated in section 2.2.

4.2. Particle acceleration in a relaxed-compressed turbulence

In the next paragraphs, we present some useful analytical estimations for the analysis of the numerical simulations presented in section 4.3. These calculations used the Heaviside related profiles derived in section 4.1.1. Let us note that the following characteristic timescales are strictly valid in the framework of *infinitely extended* diffusive zones but are used to discuss the effect of a *spatially limited* diffusive zones. However we will see in section 4.3 that these approximations lead to correct energy spectrum features, except near highest energies.

4.2.1. General statements on the turbulence parameters

Pohl et al (2005) have discussed various possible downstream relaxation processes. First, the non-linear Kolmogorov damping produces a relaxation length $\ell_d(k) \propto k^{(\beta-3)/2}$. Each turbulence mode k being in resonance with relativistic particle whose Larmor radius verifies $k\bar{r}_L \geq 1$, we obtain $\delta_d = (3-\beta)/2 \geq 0$ (between 1 and 1/2 for $1 \leq \beta \leq 2$). The two other processes considered by Pohl et al (2005) scale as $k^{-1/2}$, namely $\delta_d = 1/2$. A variation range of δ_d between 1/2 and 1 is then clearly identified. We will extend it to encompass the regime $\delta_d = 0$, a limiting case where relaxation lengths are spatially independent.

What about having δ_d negative ? A strict lower limit on δ_d is given by the condition $\ell_d(E_{CR-min}) \leq R_{sh}$. A non-relativistic minimum resonant energy $E_{CRmin} \simeq 0.1 \times (\sqrt{2} - 1)m_p c^2$ seems acceptable so that $\delta_d \geq \delta_{d,lim} = \ln(R_{sh}/\ell_{d,M})/\ln(E_{CR-min}/E_{CR-max})$. The lower limit $\delta_{d,lim}$ has typical values between -0.3 and -0.2 when identifying $\ell_{d,M}$ with the size of the X-ray filament. Relaxation regimes having $\delta_d < 0$ do not necessary correspond to any known damping process but has some interesting properties, in particular concerning the radio filaments.

4.2.2. The dominant loss mechanism

Comparing typical energy loss timescale is a useful tool to determine whether or not diffusive particle losses can affect the energy spectrum of relativistic particles. Assuming that turbulence relaxation follows a Heaviside prescription, we can express these timescales assuming constant downstream magnetic field on the relaxation length ℓ_d relativz to particle having energy E.

Four timescales are relevant in order to set the maximum particle energy in a relaxed and compressed turbulence:

1. The acceleration timescale:

$$t_{acc}(E) \simeq [7\text{ yrs}] \times \bar\rho_M \times \bar{y}(r)K(\beta, r) \times \frac{\lambda_{max,d-2}}{V_{sh,4}^2} \times \left(\frac{\rho_d(E)}{\rho_M}\right)^{2-\beta} \tag{36}$$

where $K(\beta, r) = q(\beta) \times (H(\beta, r)/r + 1)$ and where the maximum wavelength of the downstream turbulence is expressed in units of 10^{-2} pc.

2. The advection timescale: the time required for a particle to travel over a distance ℓ_d while being advected with the downstream flow.

$$t_{adv}(E) = \frac{\ell_d(E)}{V_d} \simeq [4 \text{ yrs}] \times \bar{r} \, V_{sh,4}^{-1} \ell_{d-2}(E) . \qquad (37)$$

3. The diffusive timescale: this is the time required for a particle to travel over a distance ℓ_d in a diffusive motion. [7]:

$$t_{diff}(E) = \frac{\ell_d(E)^2}{6D_d(E)} \simeq [0.3 \text{ yrs}] \times \frac{\ell_{d-2}(E)^2}{q(\beta)\bar{\rho}_M \lambda_{max,d-2}} \times \left(\frac{\rho_d(E)}{\rho_M}\right)^{\beta-2} . \qquad (38)$$

4. The synchrotron loss timescale:

$$t_{syn}(E) \simeq [1.25 \times 10^3 \text{ yrs}] \times E_{TeV}^{-1} \times B_{d-4}^{-2} \times f_{sync} . \qquad (39)$$

Parameter f_{sync} stands for $(H(\beta, r) + r)/(H(\beta, r)/r_B^2 + r)$. This expression takes into account both mean residence time in the upstream and downstream medium.

The maximum electron energy is given by the equality $t_{acc}(E_{e-max}) = t_{loss}(E_{e-max})$, where t_{loss} is the smallest timescale among synchrotron, advective and diffusive timescales. When X-ray filaments are controlled by the radiative losses, we have $t_{loss} = t_{syn}$. In case of escape losses dominated filaments, we then have $t_{loss} = \min(t_{diff}, t_{adv})$. It can be seen that fro particles having energy close to E_{e-max}, diffusive losses are always dominant compared to the advection losses, hence $t_{loss}(E_{e-max}) = t_{diff}(E_{e-max})$. It is noteworthy that the downstream residence time $t_{res,d} \simeq (V_d/c)t_{acc}$ (during one Fermi cycle) should not be compared to the diffusive or advective timescales as only particles returning to the shock are able to experiment a full Fermi cycle. Doing such comparison would lead to a maximum particle energy E_{e-max} much larger than values obtained in the context of our numerical simulations.

4.2.3. Conditions for an efficient particle acceleration

In the context of relaxation dominated filaments, the ratios of the acceleration timescale (Eq.36) to the diffusive (Eq.38) and to the advective(Eq.37) timescales vary as $E^{2(2-\beta-\delta_d)}$ and $E^{(2-\beta-\delta_d)}$ respectively. Two different regimes have now to be discussed.

$2 - \delta_d - \beta > 0$: Once $E \leq E_{e-max}$ the various timescales order as $t_{acc} \leq t_{diff}$ and $t_{acc} \leq t_{adv}$: the acceleration process can occur without noticeable losses and thus particle energy spectrum behaves as a power-law. It is noteworthy that for energy smaller than E_{adv}, advection losses become dominant compared to the diffusive losses. Formally, we derive this energy limit by setting $t_{acc}(E_{e-max}) = t_{diff}(E_{e-max})$, which leads to

$$E_{adv} = E_{e-max} \times \left(\frac{g(r)}{6}\right)^{1/2(2-\delta_d-\beta)} , \qquad (40)$$

where $g(r) = 3/(r-1) \times (H(\beta, r)/r + 1)$. We will note hereafter $\bar{g}(r) = g(r)/g(4)$.

$2 - \delta_d - \beta < 0$: In that case, the ratio of the diffusive to advective timescales is always smaller than unity, i.e. diffusive losses dominate for all energies. Once $E \leq E_{e-max}$, downstream escapes

limit the shock acceleration process considerably as the acceleration time becomes larger than t_{diff} as energy is decreasing. The same conclusion can be obtained from a close examination of the particle distribution given in Eq.(12). The term $z_d = u_d\ell_d/D_d$ is proportional to $(t_{diff}/t_{acc})^{1/2}$, and $2 - \beta - \delta_d < 0$ leads to z_d tending toward zero. The particle energy spectrum then steepens at low energy, which is obviously in complete disagreement with the Fermi acceleration scenario.

Hence, efficient Fermi acceleration is solely possible if $2 - \delta_d - \beta \geq 0$. For instance, an energy independent relaxation length $\delta_d = 0$ (as well as $\delta_d < 0$) verifies such a criterion for all diffusion regimes. In the case of a Kolmogorov type non-linear turbulence damping, the supplementary relation $\delta_d = (3-\beta)/2$ imposes $\beta \leq 1$ which means that only the Bohm regime can fulfil the previous condition (we will see in Section 4.3 that particle acceleration is not efficient in that case). In the context of Alfvén and magnetosonic cascades, Kolmogorov turbulence regime ($\beta = 5/3$) is the sole regime failing to verify the previous condition.

4.2.4. Magnetic field limits in a relaxed-compressed turbulence

In the context of X-ray filaments controlled by the downstream turbulence damping, we can link the size of the filament, noted ΔR_X, to the maximal relaxation length $\ell_{d,M}$ as $\ell_{d,M} = \Delta R_X(E_{e-max}/E_{e-obs})^{\delta_d} = C(\delta_d)\Delta R_X$. [8] The energy E_{e-obs} is the energy of particles emitting in the $4 - 6$ keV band and this value depends on the local value of the total magnetic field.

A downstream magnetic field estimation $B_{d,diff}$ can be obtained from the dynamics of the electrons by requiring that $t_{acc}(E_{e-max}) = t_{diff}(E_{e-max})$ using the previous relation between ℓ_d and ΔR_X. In the context of the Bohm diffusion, one obtains

$$B_{d,-4,diff} \simeq 3.7 \times q(\beta = 1)^{2/3} \times \left(\frac{E_{\gamma-cut,keV}^{1/2}\bar{y}(r)^{1/2}}{\Delta R_{X,-2}C(\delta_d)V_{d,3}}\right)^{2/3} , \qquad (41)$$

where $V_{d,3} = V_d/10^3$ km/s and again $\bar{g}(r) = g(r)/g(r = 4)$. If $\beta > 1$ the derivation of the magnetic field amplitude is more cumbersome.

Having the SNRs X-ray filaments dominated either by the relaxation of the downstream magnetic turbulence or by synchrotron losses is provided by the condition $t_{diff}(E_{max}) = t_{syn}(E_{max}) = t_{acc}(E_{max})$. The corresponding limit value of the magnetic field is (again in case of Bohm diffusion)

$$B_{d,-4,lim} \simeq 8.9 \times \left(\frac{V_{sh,4}}{\bar{r}\bar{g}(r)^{1/2}} \times \frac{E_{\gamma-cut,keV}^{-1/2}}{C(\delta_d)\Delta R_{x,-2}} \times f_{sync}\right)^{2/3} . \qquad (42)$$

In order to get SNRs X-ray filaments dominated by the relaxation of the magnetic field, it is compulsory to have $B_{d,diff} < B_{d,lim}$. The factor $q(\beta)$ has been isolated in expression (41) to show that no solution is then possible if $q(\beta = 1) \gg 1$. In other words, a diffusion coefficient close to the Bohm value is required to allow the relaxation of the turbulence to control the size of the

---

[7] The factor 6 in the denominator of Eq.(38) appears as the random walk along the radius of a sphere is in fact composed of 3 independent random walks along each Cartesian coordinates

[8] The dependence of ℓ_d with respect to the wavelength λ is a priori valid only up to $\lambda_{max} \simeq R_L(E_{CR-max})$ and rigorously, we should not expect the scaling of ℓ_d to extend beyond λ_{max}. Above λ_{max}, the diffusion coefficient increases as R_L^2 and particle acceleration still proceeds beyond E_{CR-max} but the number of particle accelerated and the turbulence energy density both rapidly drop. For this reason we still consider δ_d to be controlled by the kernel of the damping rate above E_{CR-max}; e.g. in the case of the Kolmogorov damping $\delta_d = 3/2$ in this energy regime.

SNR	$\dfrac{B_{d-diff}}{q(1)=1}$	$\dfrac{B_{d-diff}}{q(1)=1}$	$\dfrac{B_{d-lim}/B_{d-diff}}{q(1)=1}$	$\dfrac{B_{d-lim}/B_{d-diff}}{q(1)=16}$
Cas A	311	394	2.3	0.4
Kepler	220	293	3	0.5
Tycho	210	333	5.1	0.8
SN 1006	174	189	1.2	0.2
G347.3-0.5	164	183	0.95	0.15
	$\delta_{\mathrm{d}} = 0$	$\delta_{\mathrm{d}} = 1/2$	$\forall \delta_{\mathrm{d}}$	$\forall \delta_{\mathrm{d}}$

Table 3. Table presenting analytical estimates for the downstream magnetic field value in the context of *diffusive loss dominated* SNRs rims. The SNR rim observed parameters are the same as in Parizot et al (2006) and the shock compression ratios are $r_{\mathrm{tot}} = r_{\mathrm{sub}} = 4$.

filaments. We have also to keep in mind that the downstream magnetic field amplitude have to be coherent with the aforementioned assumption that an amplification upstream has occurred, namely $B_{\mathrm{d}} \gg B_{\mathrm{ISM}}$.

Concerning cosmic rays having energy $E \sim E_{\mathrm{CR-max}}$, the downstream diffusive losses will dominate if particles cannot escape from the upstream region into the ISM. This imposes a constraint on the magnetic field amplitude at the shock obtained from Eq.(22). Indeed, upstream escape losses are dominant if $t_{\mathrm{acc}}(E_{\mathrm{CR-max}}) < t_{\mathrm{diff}}(E_{\mathrm{CRmax}})$, using $\ell_{\mathrm{d}}(E_{\mathrm{CR-max}}) = \Delta R_{\mathrm{X}}(E_{\mathrm{CR-max}}/E_{\mathrm{e-obs}})^{\delta_{\mathrm{d}}}$.

– In case $\delta_{\mathrm{d}} = 0$, downstream diffusive escapes downstream always control the maximum CR energy.
– For $\delta_{\mathrm{d}} \neq 0$ the previous condition leads to an upper limit on the downstream magnetic field, noted $B_{\mathrm{d,esc}}$. Hence if $B_{\mathrm{d}} \geq B_{\mathrm{d,esc}}$ the CR maximum energy will be fixed by the upstream escape losses and conversely if $B_{\mathrm{d}} \leq B_{\mathrm{d,esc}}$ the CR maximum energy will be set by the downstream escape losses.

The downstream magnetic field then has to fulfil $B_{\mathrm{d,diff}} \leq \min(B_{\mathrm{d,esc}}, B_{\mathrm{d,lim}})$ in order to let the downstream turbulence relaxation be the controlling process of the energy cut-off of relativistic particles. Applying the previous conditions to our SNR sample, we always find that $B_{\mathrm{d,lim}} < B_{\mathrm{d,esc}}$. This means that an intermediary regime may exist where electrons lose their energy through radiative losses while cosmic rays cut-off is set by downstream diffusive losses. Of course, if the magnetic amplification process is efficient enough to generate higher turbulent magnetic field amplitude then upstream losses will take over.

Tab.(3) displays the values of $B_{\mathrm{d,lim}}$ and $B_{\mathrm{d,diff}}$ related to our SNR sample. The Kolmogorov regime was discarded as it does not produce any efficient acceleration as we will see in section 4.3. We show that for SN 1006 and G347.3-0.5, not much room is effectively left for the case of magnetic relaxation controlled filaments. This result seems rather robust as a variation of the shock velocity by a factor of 40%, or a variation of the synchrotron cut-off by a factor of 2 does not lead to any variation of the magnetic field larger than 25%. However a variation of the filament width by a factor of 2 would imply a variation of the magnetic field by a factor of 60% which may slightly modify the previous conclusion. Quite generally, the maximum magnetic field amplitude is found to lie in the range $\sim 200 - 300\ \mu$Gauss. In summary we find that if downstream magnetic relaxation is controlling the features of the SNRs X-ray filaments, a Bohm like diffusion regime is likely to occur while the particle diffusion coefficient normalization factor $q(\beta = 1)$ has to be quite close to unity, i.e. the diffusion regime has to be close to a genuine Bohm diffusion regime. In that context, we show that only a fraction of our SNR sample is able to achieve such consideration, namely the young ones. Indeed, using the various observational constraints related to the older SNRs (SN1006 and

G347.3-0.5), we have shown that the X-ray filaments existing in these objects are likely to be ruled by radiative losses associated with synchrotron emission.

4.2.5. Radio filaments

The energy of the radio electrons is typically four order of magnitude below the X-ray emitting electrons:

$$E_{\mathrm{eobs,R}} \simeq [1.5\mathrm{GeV}]\ B_{\mathrm{d},-4}^{-1/2} E_{\gamma-\mathrm{obs-GHz}}^{1/2},$$

where $E_{\gamma-\mathrm{obs-GHz}}$ is the energy of the radio electrons emitting in the GHz band. Using both Eq.(39) and (37), one can easily check that the synchrotron loss timescale at $E_{\mathrm{eobs,R}}$ is always larger than the advective loss timescale, unless δ_{d} is lower than typical values of the order of -0.5, a value always smaller than $\delta_{\mathrm{d,lim}}$. If $\delta_{\mathrm{d-lim}} \leq \delta_{\mathrm{d}} \leq 0$, the small turbulence scales relax on distances larger than ΔR_{X}. This very particular case would produce radio filaments larger than the size of X-ray filaments inferred from the Chandra observations. Conversely, the regime $\delta_{\mathrm{d}} \geq 0$ would let the largest fluctuating scales controlling the size of the radio filaments. In that case, the radio filaments are expected to be of the order of ΔR_{X} (see Cassam-Chenaï et al. (2007)).

4.3. Numerical simulations

We have performed MHD-SDE simulations taking into account all previous settings, namely the downstream magnetic field relaxation, the stochastic reacceleration and the radiative losses for the electrons. We discuss, in the following paragraphs, the physical agreement of assuming magnetic field relaxation to control the X-ray filaments and the actual results coming from the computation of relativistic electrons acceleration.

4.3.1. Downstream magnetic Kolmogorov damping

When non-linear Kolmogorov damping is occurring in the downstream medium of the shock, we have seen in the previous sections that two conditions have to be fulfilled to reproduce both the appropriate energy cut-off and the correct size of the observed X-ray filament. These two conditions can be transposed as: having the correct downstream magnetic field given by Eq.(41) (in order to have the electron energy cut-off consistent with the observations) and having the typical magnetic relaxation length x_{O-K} (see Eq.31) of the same order than the size of the X-ray filament. In the non-linear Kolmogorov regime, the only diffusion regime able to provide an efficient particle acceleration is the Bohm diffusion regime, where the relaxation energy index $\delta_d = 1$. Inserting, for instance in the context of the Kepler SNR, this value in Eq.(41) leads to a downstream magnetic field of the order of $B_{\mathrm{d}} \simeq 390 \mu G$ and a relaxation of the
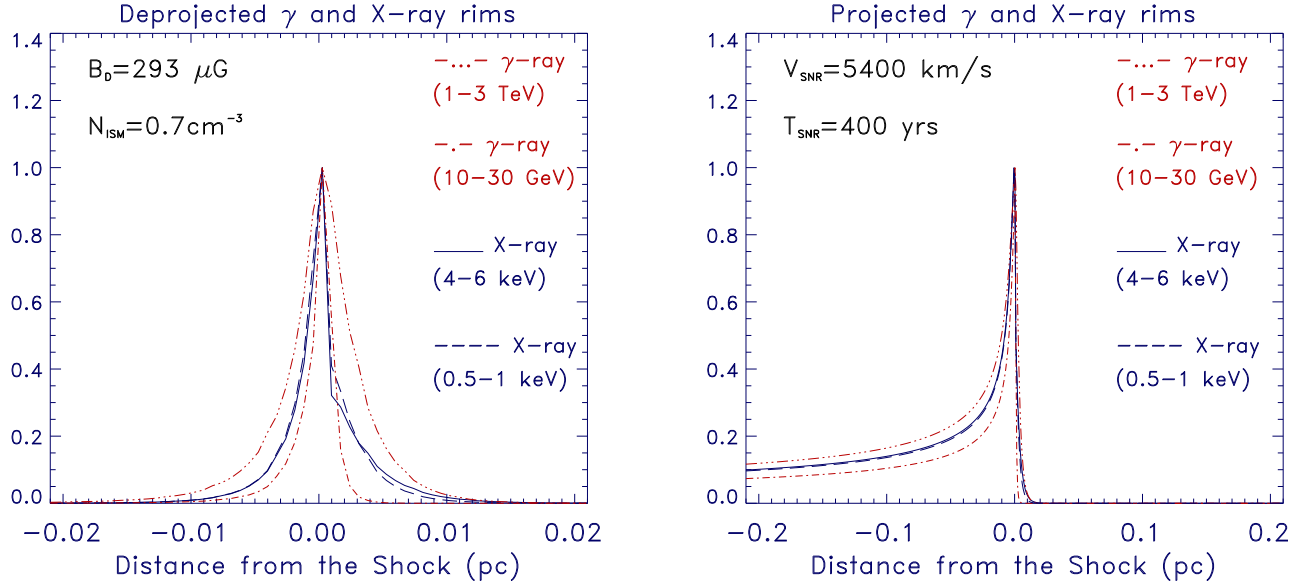
Fig. 7. The unprojected and projected X-ray and γ-ray rims in the conditions of the Kepler SNR in the case of an exponential relaxation profile. For clarity both X- and γ-ray rims have been normalised to one.
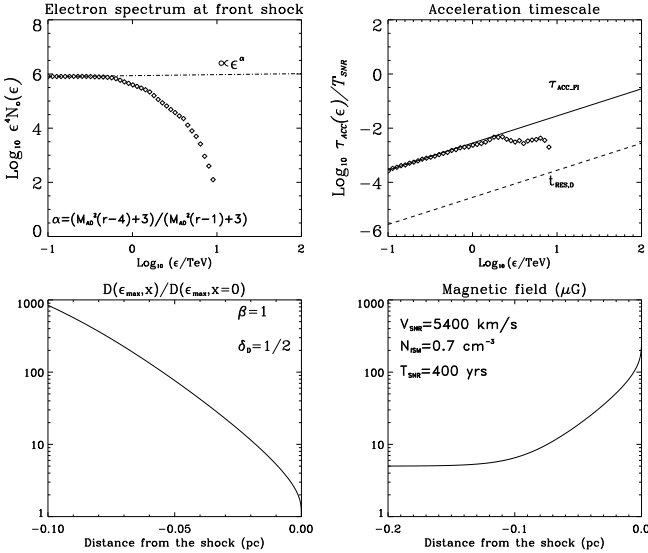

Fig. 6. Energy spectrum of relativistic electrons at the shock front given by MHD-SDE simulations in the conditions of the Kepler SNR (see Fig.2 for details). The magnetic field is damped in the downstream medium following an exponential relaxation as in Alfvènic-fast magnetsonic modes damping. Bohm regime in downstream region has been assumed. The dashed-line shows the stationary solution found in Marcowith et al (2006) which includes particle reacceleration in the Fermi cycle. In the upper right panel the acceleration (only the regular Fermi acceleration), the diffusive and downstream residence timescales are displayed using solid and dashed lines. Diamonds stand for our numerical calculation of the acceleration timescale, which is in agreement with the theoretical estimation. We also displayed in the two lower panels the spatial dependence of the diffusion coefficient at the maximum electron energy (lower left) and the magnetic profile in the downstream medium at $t = 400$ years (lower right).

order of $x_{0-K} \simeq 0.39$ pc. The relaxation size is clearly too large to provide an X-ray filament whose thickness is inferred to be of the order of 10^{-2} pc from X-ray observations. Applying the same reasoning to the other SNRs leads to a similar conclusion: having both the appropriate electron energy cut-off and X-ray

filament size is incompatible with a non-linear Kolmogorov occurring in the downstream medium of the SNR shock. The only way to overcome such conclusion would be to have the factor $\sigma = \ln(k_{max}/k_{min})$ to be much smaller than expected (see Eq.31). Anyway, having σ so small would mean that the range of particle energy able to resonate with turbulence mode would is so narrow that it would not be able to provide any significant acceleration. This explains why our result differs from the conclusion drawn by Pohl et al (2005). It seems then that it is very unlikely that non-linear Kolmogorov damping, which is a slower process compared to Alfvén/ fast magnetosonic cascade, is occurring in downstream medium of SNRs shocks.

4.3.2. Alfvènic-Fast magnetosonic modes damping

In the context of Alfvénic/ fast magnetosonic turbulence relaxation, the typical relaxation length x_{0-A} is smaller than x_{0-K}. Indeed, compiling the aforementioned necessary conditions to reproduce accurately X-ray filament in the SNR environment, we get typical x_{0-A} of the order of 10^{-2} pc when using magnetic field values provided by Tab.(2). This means that the Alfvénic / fast magnetosonic modes damping is a plausible candidate to explain the presence of SNRs X-ray filaments. In order to sustain this conclusion, we have performed, in the context of the Kepler SNR, MHD-SDE simulations aiming to reproduce the dynamics of relativistic electrons and the associated X-ray and γ-ray emission maps. In Fig.6 and Fig.7, we have displayed the particle distribution at the shock front and the X- and γ-ray filaments respectively. All simulations have been performed in the Bohm regime. In that case $2 - \delta_d - \beta = 1/2 > 0$.

Several tricking differences appear in both Fig.6 and Fig.7 with respect to the simple advection case presented in Fig.2 and Fig.3. First as stated in section 4.2 the normalization of the diffusion coefficient $q(\beta)$ has to be close to one. Even in this case, the maximum particle energy is limited to values close to ten TeV (for parameters associated with the Kepler SNR). One of the necessary condition to fit the observed size of the X-ray rim, namely $x_{0-A} \sim \Delta R_X$ lead to an increase of the diffusion coefficient by a factor of the order of a few tens over the typical
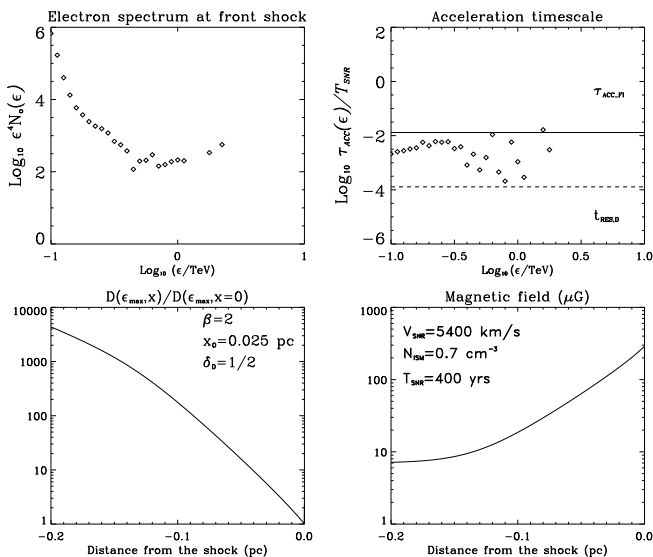
Fig. 8. Same case as treated in Fig.6 but with $\beta = 2$. Here, massive diffusive losses are occurring since $2 - \delta_d - \beta < 0$ and thus no significant acceleration is observed.

diffusion length, implying low maximal energies for both electrons and cosmic rays. The X- and γ-ray filaments also display some different features in the case of an Alfvènic-like relaxed turbulence. Indeed, the low energy particles producing the synchrotron photons in the interval 0.5-1 keV and the γ-ray photons in the 10-30 GeV band respectively do extend over smaller distances behind the shock (electrons having energy ~ 1 TeV). This can be understood by the effect of the resonant component of the magnetic field b in Eq.(6). At a given downstream location, particles with energies $E < E_{max}$ do interact with a smaller number of modes compared to the advected case. This effect is due to the fact that large wave numbers modes relax over smaller distances compared to smaller wave numbers modes within the same turbulence spectrum. In other words, when comparing to the advected case, more low energy particles suffering diffusive losses are lost compared to the highest energies (which also suffer from diffusive losses). Particles having energy around a few tens to hundred of GeV are then confined closer to the shock and do not experience a strong magnetic field variation: the standard shock solution is then recovered in this domain. We have checked that the shock synchrotron spectrum cuts off at an energy near one keV.

We also have tested the solution in the case $\beta = 2$; i.e. $2 - \delta_d - \beta = -1/2 < 0$. No significant particle acceleration has been found as diffusive losses dominate at low energy (see Fig.8). The numerical acceleration timescale is also found to be smaller to the theoretical estimation which is consistent with the fact that only particles returning quickly to the upstream medium once entering the downstream region are able to avoid massive diffusive losses. These simulations confirm the conclusions drawn in section 4.2.3.

4.3.3. Solutions in case of turbulent dynamo amplification

The coherence length of the downstream turbulence entering the evaluation of ℓ_{ampl} in section 4.1.4 cannot be larger than the X-ray filament width otherwise the condition on the maximum CR diffusion coefficient upstream given by the Eq.(22) would not be satisfied. This means that if a magnetic dynamo operates downstream then the growth scale length is $< \Delta R_X$. The

growing modes are restricted mostly to large scales; i.e. to wave numbers close to k_{min}. They are considered by the particles as a contribution to the mean magnetic field. The fast increase of the magnetic field downstream up to values close to equipartition produces enhanced radiative losses and thus much thinner filaments. We have checked the effect by performing simulations adding a mean magnetic field downstream with values close to a few mGauss.

5. Discussion and summary

Young SNRs are strong particle accelerators as probed by the presence of thin X-ray filaments. In these astrophysical objects, the X-ray emission is produced by synchrotron radiation, involving particle whose maximal energy is beyond tens of TeV and magnetic field strengths behind the shock of the order of a few hundred μGauss (Parizot et al 2006). This work extends the examination undertaken by Parizot et al (2006) about the physical properties of the turbulence and transport coefficients in the same sample of five young SNR. We have further included the turbulence compression at the shock front, the possibility of particle reacceleration in the downstream region of the shock and finally the relaxation of the magnetic fluctuations downstream (Pohl et al 2005). We have also included a description of the generation of the magnetic fluctuations in the shock precursor following the two regimes of the streaming instability (Pelletier et al 2006). This work has been developed in the same framework as Lagage & Cesarsky (1983) but adapted to the case of amplified magnetic field around SNR, except that the maximum CR energy is not fully investigated here. For that purpose we have developed a numerical scheme based on the coupling between the equations of the magnetohydrodynamics and a kinetic scheme handling the calculation of the electrons particle distribution function. The scheme involves a set of stochastic differential equations (SDE) already described elsewhere (Casse & Marcowith 2003, 2005). The SDEs have been adapted to account for the discontinuity of the diffusion coefficients properly using a skew brownian motion (see also Zhang (2000)). The following conclusions can be made:

1. The compression of turbulent scales at the shock front does not deeply modify the efficiency of shock acceleration. The conclusions addressed by Parizot et al (2006) are found to be robust; in case of downstream advected magnetic field, young SNRs exhibiting X-ray filaments do accelerate particles at most at PeV energies.
2. Considering the various regimes of the streaming instability occurring in the shock precursor, the SNRs contained in our sample are expected to generate magnetic fields up to a few hundred μGauss. In a regime of shock velocity of a few hundred thousand km/s the level of fluctuations tend to be shared by the non-resonant and the resonant regimes. The resonant modes may contribute to some particle reacceleration downstream. However the amount of reacceleration cannot be too large otherwise the shock particle spectrum would be harder and the X-ray filament width would be larger than observed. This provides an observational constraint on the amount of resonant modes present downstream of the shock front. The fate of non-resonant modes generated upstream still requires specific developments.
3. We provided calculations of the projected and deprojected X- and γ-ray filaments, each one in two specific wavebands. If the separation between the X and γ-ray peak emission is found to be far below any γ-ray mission resolution capacities

in young SNR, some detailed observations could be undertaken in the case of more extended objects like Vela Junior.

4. In the case of a relaxed turbulence occurring in the downstream region, our conclusions are the following:

   – When the magnetic relaxation scale varies as $\ell_d(k) \propto k^{-\delta_d}$, a magnetic turbulence (whose power-law index is β) is able to provide suitable conditions giving rise to an efficient particle acceleration if $2 - \delta_d - \beta > 0$.

   – We have put to the test several relaxation processes leading to various values of δ_d. It appeared that the Kolmogorov damping occurring in a Bohm diffusion regime is unlikely to produce strong acceleration in the framework of relaxation limited filaments when accounting for the whole dynamics of the turbulent spectrum. On the other hand, the Alfvén and fast magneto-sonic cascades provide suitable conditions giving birth to particle acceleration while being able to match all observational features of X-ray filaments. In that context, we found that the maximum energy particle (both for electrons and cosmic rays) cannot be much larger than a few tens of TeV.

   – The magnetic field strengths downstream of the shock cannot be much larger than $200 - 300 \mu$ Gauss otherwise radiative losses would control the X-ray filament width.

   – Regarding the supernova remnants SN1006 and RXJ 1713-3946.5, none of the various turbulence relaxation processes considered in the present paper were able to provide an efficient particle acceleration and to match the corresponding observational features. In that context, it seems that only the youngest SNRs ($T_{SNR} < 500$ yr) of our sample may exhibit X-ray filaments controlled by downstream turbulence relaxation.

   – The normalization (i.e. factor $q(\beta)$) of the spatial diffusion coefficient have to remain close to unity in order to avoid massive particle diffusive losses, leading to a drop of the Fermi acceleration efficiency. A genuine Bohm diffusion regime is then required if magnetic turbulence relaxation is occurring in the downstream region of the shock.

Appendix A: Magnetic field profile produced by the resonant instability

The amplification factor due to the resonant instability depends on the amplification factor produced by the non-resonant instability (Pelletier et al (2006), Eq.34); it reads as:

$$A_R^2(x) = \tilde{\alpha}_{res} \times A_{NR}(x) \times \int_1^{k_* \ell_{coh}} d\ln(\bar{k}) \left(\exp(-a(x)\bar{k}^{2-\beta}) - 1/e \right) , \tag{A.1}$$

and $\tilde{\alpha}_{res} = \pi/\phi \times M_{A\infty} \xi_{CR} > 1$ and k_* is the maximum resonant wave length at a distance x.
$\bar{k} = k\ell_{coh}$ varies between $k_{min}(= 1/r_L(E_{CR-max}))\ell_{coh} \simeq 1$ and $k_*(x)\ell_{coh} \geq 1$ [9]. We have:

$$a(x) = \frac{\pi}{\beta\phi} \times (V_{sh}/c) \times (x/\ell_{coh}) \times \eta_{tot}(x) < 1 ,$$

---

[9] As discussed in section 2.1.1 we assume the same coherence length over the whole precursor.

The exact integration of Eq.(A.1) involved a difference between two exponential integral: $Ei(-a(x)\bar{k}_*) - Ei(-a(x))$. The second term dominates as $\bar{k}_* \geq 1$, we get:

$$A_R(x) \propto \left[A_{NR}(x) \times (-Ei(-a(x))/(2 - \beta) - \ln(k_*(x))/\exp(1)) \right]^{1/2} . \tag{A.2}$$

The above equation is implicit as the total magnetic field is hidden in k_* and η_{tot}.
At distances $x \ll \ell_{diff}(E_{CR-max})$, $a(x) \ll 1$, we approximate $-Ei(-a(x)) \simeq -\ln(a(x)) - C$; $C \simeq 0.5772$ is the Euler constant. At a first approximation within the precursor $A_R(x)$ scales as $A(x)_{NR}^{1/2}$.

Appendix B: Derivation of the shock particle distribution function

The steady-state general 1D Fokker-Planck equation reads:

$$u\frac{\partial f}{\partial x} = \frac{\partial}{\partial x}\left(D\frac{\partial f}{\partial x} \right) + (u_d - u_u)\delta(x)\frac{\partial f}{\partial \ln p^3} \tag{B.1}$$

Here the upstream medium is defined by $-\ell_u(p) \leq x < 0$ and the downstream medium by $0 < x \leq \ell_d(p)$. The shock front is at $x = 0$. In this equation, we have neglected the synchrotron/turbulence generation losses since we focus on the particle diffusive losses. The presence of finite extension for both upstream and downstream media imposed boundary conditions for f as $f(-\ell_u, p) = 0 = f(\ell_d, p)$. In order to determine the spatial behaviour of the f function, we integrate Eq.(B.1) from the left boundary to x in the upstream medium and from x to the right boundary in the downstream medium; we obtain:

$$f_u(x, p) = f_S(p)\frac{\int_{-\ell_u}^x \exp(\int_{-\ell_u}^{x'} \theta_u(x'', p)dx'')dx'}{\int_{-\ell_u}^0 \exp(\int_{-\ell_u}^x \theta_u(x', p)dx')dx}$$

$$f_d(x, p) = f_S(p)\frac{\int_x^{\ell_d} \exp(-\int_{x'}^{\ell_d} d(x'', p)dx'')dx'}{\int_0^{\ell_d} \exp(-\int_x^{\ell_d} \theta_d(x', p)dx')dx} \tag{B.2}$$

where f_S is the distribution function evaluated at the shock front and the functions $\theta_{u/d}$ are to be interpreted as the inverse of effective diffusive lengths and are defined as

$$\theta_{u/d}(x, p) = \frac{u_{u/d} - \frac{\partial D_{u/d}}{\partial x}}{D_{u/d}} . \tag{B.3}$$

The energy flux carried by the relativistic particle has to be conserved throughout the shock front, namely for $v \to 0$

$$\left[D\frac{\partial f}{\partial x} + u\frac{\partial f}{\partial \ln p^3} \right]_{-v}^v = 0 . \tag{B.4}$$

The spatial derivatives of f are known using Eq.(B.2); we obtain a differential equation for f_S:

$$\frac{d\ln f_S(p)}{d\ln p} = -\frac{3}{(u_u - u_d)} \times \left\{ \frac{D_u(0, p)\exp(\int_{-\ell_u}^0 \theta_u(x', p)dx')}{\int_{-\ell_u}^0 \exp(\int_{-\ell_u}^x \theta_u(x', p)dx')dx} + \frac{D_d(0, p)\exp(-\int_0^{\ell_d} \theta_d(x', p)dx')}{\int_0^{\ell_d} \exp(-\int_x^{\ell_d} \theta_d(x', p)dx')dx} \right\} . \tag{B.5}$$

Appendix C: Particle acceleration and multi-scale simulations

This section presents the numerical framework used to describe both the supernova thermal plasma evolution and the relativistic charged particles transport. As detailed in Casse & Marcowith (2003) and Casse & Marcowith (2005), the background fluid and large scale-magnetic field are calculated using the magnetohydrodynamics code VAC for *Versatile Advection Code* (Tóth (1996)). The simulations are performed using a 1D spherical symmetry where the evolution of the supra-thermal electrons and nuclei are calculated using the stochastic differential equations (SDE) formalism (Krülls & Achterberg 1994). The numerical description of supra-thermal particles transport is crucially dependent on the ability of the MHD code VAC to capture the shock structure. In order to obtain the sharpest shock front possible, we used the TVD-MUSCL scheme coupled with a Roe-type approximate Riemann solver (Tóth & Odstrcil (1996)).

Section C.1 briefly reports on the MHD-SDE schemes used to model a 1D spherical SN remnant expansion. In particular sections C.2 and C.2.1 discussed in some details the stochastic differential Euler schemes with spatially dependent diffusion coefficients and their application to the diffusive shock acceleration problem. Section C.2.2 describes the shock capturing procedure that efficiently couple the MHD and SDE schemes.

C.1. Supernova remnants modelling

The time evolution of the thermal magnetised plasma is fully controlled by the MHD equations providing mass, momentum and energy conservation as well as electromagnetic field induction, namely

$$
\begin{aligned}
&\frac{\partial \rho}{\partial t} + \nabla \cdot (\rho \mathbf{V}) = 0 \,, \\
&\frac{\partial (\rho \mathbf{V})}{\partial t} + \nabla \cdot [\rho \mathbf{VV} + p_{tot} I - \mathbf{BB}/\mu_o] = 0 \,, \\
&\frac{\partial e}{\partial t} + \nabla \cdot \left(e\mathbf{V} + p_{tot}\mathbf{V} - \mathbf{V} \cdot \frac{\mathbf{BB}}{\mu_o} \right) = 0 \,, \\
&e = \frac{\rho \mathbf{V}^2}{2} + \frac{\mathbf{B}^2}{2\mu_o} + \frac{P}{\gamma - 1} \\
&\frac{\partial \mathbf{B}}{\partial t} + \nabla \cdot (\mathbf{VB} - \mathbf{BV}) = 0
\end{aligned}
\tag{C.1}
$$

The density ρ, velocity $\mathbf{V}$, total energy e and magnetic field $\mathbf{B}$ are set in the initial condition as a 1D spherically symetric SNR blast-wave as described by Truelove & McKee (1999). We assumed a uniform SNR and we have added a small contribution of the magnetic field. The resulting SNR MHD simulation starts as ($V_\theta, V_\phi = 0$)

$$
\rho = \begin{cases} 3M_{\mathrm{SNR}}/\rho_\infty 4\pi V_{\mathrm{SNR}}^3 T_{\mathrm{SNR}}^3 & , R < V_{\mathrm{SNR}} T_{\mathrm{SNR}} \\ 1 & , R > V_{\mathrm{SNR}} T_{\mathrm{SNR}} \end{cases}
$$

$$
V_{\mathrm{R}} = \begin{cases} R/V_{\mathrm{SNR}} T_{\mathrm{SNR}} & , R < V_{\mathrm{SNR}} T_{\mathrm{SNR}} \\ 0 & , R > V_{\mathrm{SNR}} T_{\mathrm{SNR}} \end{cases}
$$

For each run the physical quantities entering the problem are normalised knowing the mass ejected M_{SNR}, the age of the SNR T_{SNR}, the mechanical energy of the explosion E_{inj} and the velocity of the blast wave V_{NR}. We set the thermal pressure to a small value compared to the kinetic energy of the SNR (typically 10^{-3} times) since its role in the wave propagation is minimal. The magnetic field advected along the flow is also believed

to be very ineffective in the wave propagation but its role in the supra-thermal particles transport process is important. The magnetic field is thus prescribed with an amplitude similar its warm interstellar medium value e.g. $B_\theta \simeq 5\mu G$.

In order to test the ability of our simulation to model the propagation of SNR shock, we have ran a long-term evolution of a SNR blast wave corresponding to the previous initial setup where we have set the SNR parameter to $M_{\mathrm{SNR}} = 6M_\odot$, $T_{\mathrm{SNR}} = 200\mathrm{yr}$, $E_{\mathrm{inj}} = 10^{51}\mathrm{ergs}$ and $V_{\mathrm{SNR}} = 5000\mathrm{km/s}$. The results have been found to reproduce the corresponding analytical solution in Truelove & McKee (1999) quite accurately. In particular both free expansion and Sedov self-similar regime are obtained, the transition regime occurs at the expected Sedov time for this simulation, $T_{\mathrm{SEDOV}} = 1.1\mathrm{kyr}$.

C.2. Kinetic approach

The transport of relativistic particles (with velocities much larger than the fluid speed) near the shock front is governed by a Fokker-Planck equation in the case where these particles resonate with the turbulence and enter a diffusion regime. The related kinetic equation is

$$
\begin{aligned}
\frac{\partial F}{\partial t} = &- \frac{\partial}{\partial R}\left(F\left\{ V_R + \frac{\partial D_R}{\partial R} + \frac{2D_R}{R} \right\} \right) \\
&- \frac{\partial}{\partial p}\left(F\left\{ -\frac{p}{3}\nabla \cdot \mathbf{V} + \frac{1}{p^2}\frac{\partial p^2 D_{pp}}{\partial p} - a_{loss}p^2 \right\} \right) \\
&+ \frac{\partial^2}{\partial R^2}(FD_R) + \frac{\partial^2}{\partial p^2}(FD_{pp})
\end{aligned}
\tag{C.2}
$$

with $F = R^2 p^2 f$ related to the distribution function f via the spherical radius R and particle momentum $pc = \gamma m_e c^2$. The particle spatial diffusion regime is characterised by a diffusion coefficient D_R which depends on the turbulence spectrum. The factor a_{loss} stands for particle losses.

For electrons the losses are produced by synchrotron cooling. The cooling timescale t_{syn} is:

$$
a_{\mathrm{syn}} = \frac{1}{t_{\mathrm{syn}}p} = \frac{6\pi m_e^2 c^2}{\sigma_{\mathrm{T}} c B^2}
\tag{C.3}
$$

For protons (or ions) the losses are produced by the generation of magnetic fluctuations and are a priori limited to the upstream medium (in the downstream flow the particle distribution is isotropic). The cooling timescale is obtained from (Marcowith et al (2006), Eq.13):

$$
a_{\mathrm{turb}} = \frac{P(p)}{p^2} \,,
\tag{C.4}
$$

where $P(p)$ is the rate of energy radiated by a relativistic particle:

$$
P(p) \simeq \frac{1}{3}V_{\mathrm{sc}}\frac{\partial \log(f(x))}{\partial x}p \,.
\tag{C.5}
$$

The scattering center velocity is close to the local Alfvén velocity; i.e. $V_{\mathrm{sc}} \simeq V_{\mathrm{Au}}$.

Stochastic particle acceleration is represented by the energy diffusion coefficient $D_{\mathrm{pp}} = V_{\mathrm{A}}^2 p^2 / 9D_{\mathrm{R}}$ related to spatial diffusion (V_{A} is the local Alfvèn velocity).

C.2.1. Stochastic differential equations

As shown by Krülls & Achterberg (1994), this Fokker-Planck equation is equivalent to a set of two SDEs that can be written as

$$\frac{dR}{dt} = V_{\mathrm{R}} + \frac{\partial D_{\mathrm{R}}}{\partial R} + \frac{2D_{\mathrm{R}}}{R} + \frac{dW_{\mathrm{R}}}{dt}\sqrt{2D_{\mathrm{R}}}$$

$$\frac{dp}{dt} = -\frac{p}{3}(\nabla \cdot \mathbf{V}) + \frac{1}{p^2}\frac{\partial p^2 D_{\mathrm{pp}}}{\partial p} - a_{\mathrm{loss}}p^2 + \frac{dW_{\mathrm{P}}}{dt}\sqrt{2D_{\mathrm{pp}}}$$

where the W_i are Wiener processes such that $dW_i \propto \sqrt{dt}$. Using Monte-Carlo methods, it is then possible to time-integrate the trajectories of a sample of test particles in phase space and to reconstruct the distribution function provided that the number of test particles is sufficiently high.

The presence of a shock discontinuity may lead, according to MHD Rankine-Hugoniot conservation laws, to a discontinuous magnetic field at the shock front. Depending on the diffusion regime affecting relativistic particles, this may lead to discontinuous diffusion coefficients that can be written $D_{\mathrm{R}} = D_{\mathrm{R,C}} + \Delta D_{\mathrm{R}}\mathrm{sign}(R - R_{\mathrm{sh}})$ where the first term is a continuous function. In this case, the usual Euler schemes are no longer valid as in Krülls & Achterberg (1994); Casse & Marcowith (2003); van der Swaluw & Achterberg (2004); Casse & Marcowith (2005). As shown by Zhang (2000), it is possible to overcome this problem by employing a skew brownian motion where an asymmetric shock crossing probability is considered. In this framework, the spatial stochastic equation becomes

$$d\tilde{R} = \xi(\tilde{R})\left\{\left(V_{\mathrm{R}} + \frac{\partial D_{\mathrm{R,C}}}{\partial R}\right)dt + \sqrt{2D_{\mathrm{R}}}dW_{\mathrm{R}}\right\} \quad (C.6)$$

where $\tilde{R}$ is related to R by

$$\tilde{R} = \xi(R)R \quad \text{with} \quad \xi(R) = \begin{cases} \varepsilon, & R < R_{\mathrm{sh}} \\ \frac{1}{2}, & R = R_{\mathrm{sh}} \\ (1-\varepsilon), & R > R_{\mathrm{sh}} \end{cases}$$

and where ε is the ratio of diffusion coefficients taken at the shock front, namely

$$\varepsilon = \frac{D_{\mathrm{u}}(R_{\mathrm{sh}})}{D_{\mathrm{u}}(R_{\mathrm{sh}}) + D_{\mathrm{d}}(R_{\mathrm{sh}})}. \quad (C.7)$$

Eq. (C.6) can be solved using an Euler scheme where the stochastic variable W_R is computed with Monte-Carlo methods. Conversely to the study of Zhang (2000), realistic diffusion coefficients are likely to depend on particle energy. In this case we have to consider the amount of energy $\Delta\epsilon$ gained by particles during the shock crossing. The transition probability ε is then calculated depending on the way the shock is crossed, namely

$$\varepsilon_{up\to down} = \frac{D_{\mathrm{u}}(R_{\mathrm{sh}}, \epsilon)}{D_{\mathrm{u}}(R_{\mathrm{sh}}, \epsilon) + D_{\mathrm{d}}(R_{\mathrm{sh}}, \epsilon + \Delta\epsilon)}$$

$$\varepsilon_{down\to up} = \frac{D_{\mathrm{u}}(R_{\mathrm{sh}}, \epsilon + \Delta\epsilon)}{D_{\mathrm{u}}(R_{\mathrm{sh}}, \epsilon + \Delta\epsilon) + D_{\mathrm{d}}(R_{\mathrm{sh}}, \epsilon)}. \quad (C.8)$$

It is noteworthy that this skew brownian motion approach is valid only if shock curvature terms are neligeable, i.e. $2D_{\mathrm{R}}/R \ll |V_{\mathrm{R}} + \partial D_{\mathrm{R}}/\partial R|$. Regarding the energy stochastic equation, the velocity discontinuity can be numerically treated by an implicit Ricatti scheme (Marcowith & Kirk 1999). Basically, once the stochastic displacement ΔR is calculated, we can calculate the energy gained $\Delta\epsilon$ by a particle having originally an energy $\epsilon = pc$ during time step Δt following

$$\frac{\epsilon + \Delta\epsilon}{\epsilon} = \frac{\exp\left(-\frac{\Delta t}{3\Delta R}\int_R^{R+\Delta R}\nabla \cdot \mathbf{V}dR\right)}{1 + \epsilon\exp\left(-\frac{\Delta t}{3\Delta R}\int_R^{R+\Delta R}\nabla \cdot \mathbf{V}dR\right)\frac{\Delta t}{\Delta R}\int_R^{R+\Delta R}a_{\mathrm{loss}}dR} \quad (C.9)$$

The previous implicit calculation is valid for any diffusion regime provided that second order Fermi acceleration is negligeable. In the opposite case, we then have to step back into an explicit scheme taking into account the skew brownian motion. Following Zhang (2000) the energy gained by a particle will be

$$\Delta\epsilon = \sqrt{2D_{\mathrm{pp}}}dW_{\mathrm{p}} - \frac{\Delta V}{3\Delta D_{\mathrm{R}}}\epsilon\{\Delta \mathrm{R} - \Delta\tilde{R}/\xi(\tilde{R})\} + \left(\frac{\partial D_{\mathrm{pp}}}{\partial p} - a_{\mathrm{loss}}\right)\Delta t \quad (C.10)$$

where $\Delta V = V_{\mathrm{up}}(R_{\mathrm{sh}}) - V_{\mathrm{down}}(R_{\mathrm{sh}})$ and $\Delta D_R = D_{\mathrm{u}}(R_{\mathrm{sh}}) - D_{\mathrm{d}}(R_{\mathrm{sh}})$. During the time integration of MHD equations, the SNR shock front is propagating so that its surface is increasing with time. In order to take into account the increase of the particle flux at the shock front, we continuously inject new particles having energy ϵ_{inj} so that the number of new particles is $N_{\mathrm{part}}(t+\Delta t) - N_{\mathrm{part}}(t) \propto R_{\mathrm{sh}}^2(t)\Delta R_{\mathrm{sh}}$, where ΔR_{sh} is the shock front displacement occurring during Δt.

C.2.2. Kinetic description of MHD shock waves

The SDE formalism is useful to model the transport of relativistic test particles in the context of a non-relativistic background fluid since it provides both spatial and energetic distribution of particles. Nevertheless one drawback of this method does exist: the shock thickness. Indeed the SDE algorithm is based on the use of fluid velocity divergence to mimic particle acceleration. The MHD code is providing the velocity field at discrete locations on the grid so that $\nabla \cdot \mathbf{V}$ may be obtained through linear interpolation. The best performant MHD code cannot display shocks as sharp discontinuities but rather display velocity and density variations over two or three cells. This is very important for kinetic computations since particles having diffusion coefficients such that the diffusive step is small than the MHD shock thickness will see the shock as an adiabatic compression, leading to softer energy spectrum.

In previous works (see e.g. Krülls & Achterberg (1994); Casse & Marcowith (2003), it was shown that the SDE formalism was able to describe accurately the transport of particles having diffusion coefficients larger than $\Delta X_{\mathrm{sh}}V/2$ where ΔX_{sh} is typically the cell size in the MHD code. This constraint greatly reduced the range of applications of this method. In order to overcome this problem, we have designed a SDE algorithm where the $\nabla \cdot \mathbf{V}$ is no longer calculated locally but instead we integrate the term $\nabla \cdot \mathbf{V}dR$ in Eq.(C.9) where the velocity is given as V_{u} or V_{d} depending on the shock position. In our new approach, the MHD code is now only providing the shock position and the compression ratio r so that we deduce the value of the fluid by considering the shock as infinitely thin.

References

Acero, F., Ballet, J. & Decourchelle, A. A&A, 475, 883
Aharonian, F.A. et al. 2004, Nature, 432, 75
Aharonian, F.A. et al. 2006, Nature, 432, 75
Aharonian, F.A. et al, 2008, A&A, 488, 219
Albert, J. et al, ApJ, 664, L87
Amato, E. & Blasi, P. 2009, MNRAS, 392, 1591

Ballet, J. 2006, AdSpR, 37, 1902
Bamba, A., Yamazaki, R. & Hiraga, J.S., 2005a, ApJ, 632, 294
Bamba, A., Yamazaki, R., Yoshida, T. & Koyama, K., 2005b, ApJ, 621, 793
Bamba, A. et al., 2006, AdSpR, 37, 1439
Bell, A. & Lucek, S., 2001, MNRAS, 321, 433
Bell, A.R. 2004, MNRAS, 353, 550
Berezhko, E.G., 2008, Adv.Sp.Res., 41, 429
Berezhko, E.G., Ksenofontov, L.T. & Völk, H.J., 2006, A&A, 452, 217
Berezhko, E.G., Ksenofontov, L.T. & Völk, H.J., 2003a, A&A, 412, 11
Berezhko, E.G., Pühlhofer, G. & Völk, H.J., 2003b, A&A, 400, 971
Berezhko, E.G. & Ellison, D.C., 1999, ApJ, 526, 385
Berezhko, E.G.,Elshin, V. K., Ksenofontov, L. T., 1996, JETP, 82, 1
Blumenthal, G.R., & Gould, R.J., 1970, RMP, 42, 237
Bykov, A., 2001, SSR, 99, 321
Bykov, A., 2004, AdSpR, 33, 366
Bykov, A. & Toptyghin, I.N., 2005, AstL, 31, 748
Campeanu, A. & Schlickeiser, R., 1992, A&A, 263, 413
Candia, J. & Roulet, E., 2004, JCAP, 10, 007
Cassam-Chenaï G., Decourchelle, A., Ballet, J., Hwang, U., Hughes, J. P., Petre,
    R.et al.et al., 2004, A&A, 414, 545
Cassam-Chenaï G., Hughes, J. P., Ballet, J., Decourchelle, A., 2007, 665, 315
Casse, F., Lemoine, M. & Pelletier, G., 2002, Phys. Rev. D, 65, 3002
Casse, F. & Marcowith, A. 2003, A&A, 404, 405
Casse, F. & Marcowith, A. 2005, Aph, 23, 31
Caprioli, D., Blasi, P., Amato, E., Vietri, M. 2008a, ApJ, 679, L139
Caprioli, D., Blasi, P., Amato, E., 2008b, 2008arXiv0807.4259
Diamond, P.H. & Malkov, M.A., 2007, ApJ, 654, 252
Drury, L.O'C., 1983, Rep. Prog. Physics, 46, 973
Ellison, D.C. & Vladimirov, A., 2008, ApJ, 673, L47
Goldreich, P. & Sridhar, S., 1995, ApJ, 438, 763
Giacalone & Jokipii, 1999, ApJ, 520, 204
Gotthelf, E.V., Koralesky, B., Rudnick, L., Jones, T.W., Hwang, U.& Petre, R.,
    2001, ApJ, 522, 39
Green, D.A., 2006, http://www.mrao.cam.ak.uk/surveys/snrs/
Hughes, J.P., 2000, ApJ, 545, L53
Hwang, U., Decourchelle, A., Holt, S.S. & Petre, R., 2002, ApJ, 581, L101
Kang, H. & Jones, T.W., 2007, Aph, 28, 232
Katz, B. & Waxman, E., 2008, JCAP, 1, 18
Katz, B., Keshet, U. & Waxman, E., 2007, ApJ, 655, 375
Krülls, W.M. & Achterberg, A. 1994, A&A, 286, 314
Lagage, P.-O. & Cesarsky, C.J., 1983, A&A, 118, 223
Lucek, S. & Bell, A.R. 2000, MNRAS, 314, 65
Malkov, M.A. & Diamond, P.H., 2006, ApJ, 642, 244
Marcowith, A., Lemoine, M. & Pelletier, G., 2006, A&A, 453, 193
Marcowith, A. & Kirk, J.G. 1999, A&A, 347, 291
MacKenzie, J. F.& Völk, H. J., 1982, A&A, 116, 191
Morlino, G., Amato, E. & Blasi, P., 2008, 2008arXiv0810.0094
Niemiec, J., Pohl, M., T. Stroman & K.-I., Nishikawa, 2008, ApJ, 684, 1174
Ostrowski, M. & Schlickeiser, R., 1996, SoPh, 167, 3810
Parizot, E., Marcowith, A., Ballet, J. & Gallant, Y.A., 2006, A&A,
Pohl, M., Yan, H.& Lazarian, A., 2005, ApJ, 626, 101
Pelletier, G., Lemoine, M. & Marcowith, A. 2006, A&A, 453, 181
Pelletier, G., Lemoine, M. & Marcowith, A., 2009, MNRAS, 393, 587
Ptuskin, V.S. & Zirakachvili, V.N., 2003, A&A, 403, 1
Reynolds, S.P., 1998, ApJ, 493, 375
Reville, B., Kirk, J. G., Duffy, P., O'Sullivan, S., 2007, A&A, 475, 435
Reville, B., O'Sullivan, S., Duffy, P.& Kirk, J.G., 2008, MNRAS, 386, 589
Riquelme, M.A. & Spitkovsky, A., 2009, ApJ, 694, 626
Rho, J., Dyer, K.K., Borkowski, K. & Reynolds, S.P., 2002, ApJ, 581, 1116
Shalchi, A., 2009, Aph, 31, 273
Skilling. J., 1975, MNRAS, 172, 557
van der Swaluw, E. & Achterberg, A., 2004, A&A, 421, 1021.
Takahashi, T., Tanaka, T., Uchiyama, Y., Hiraga, J. S., Nakazawa, K. et al, 2008,
    PASJ, 60, 131
Tóth, G. 1996, Astrophys. Lett. Commun., 34, 245
Tóth, G. & Odstrcil D. 1996, J. Comp. Phys., 128, 82
Truelove, J.K. & McKee, C.F. 1999, ApJS, 120, 299
Uchiyama, Y., Aharonian, F.A. & Takahashi, T., 2003, A&A, 400, 567
Vainio R. & Schlickeiser, R., 1999, A&A, 343, 303
Vink, J. & Laming, J.M., 2003, ApJ, 584, 758
Vink, J., 2004, Nucl. Phys. B Proc. Supp., 132, 21
Völk, H.J., Berezhko, E.G. & Ksenofontov, L.T., 2005, A&A, 433, 229
Vladimirov, A., Ellison, D.C. & Bykov, A., 2006, ApJ, 652, 1246
Vladimirov, A., Ellison, D.C. & Bykov, A., 2008, ApJ, 688, 1094
Weisskopf, M.C. & Hughes, J.P., 2006, Astrophysics update 2, astro-ph/0511327
Zhang, M. 2000, ApJ 541, 428
Zirakashvili, V.N. & Aharonian, F. 2007, A&A, 465, 695
Zirakashvili, V.N. & Ptuskin, V.S., 2008, ApJ, 678, 939